NASA CONTRACT NAS W 1438
REPORT NO. GDC DCL 67-002

FEASIBILITY STUDY OF LARGE SPACE ERECTABLE ANTENNAS

VOLUME III • SUMMARY

Parabolic Expandable Truss Antenna Experiment

22 January 1968

NASA/MSFC Program Manager - E. C. Hamilton
Convair Program Manager - J. A. Fager

Prepared for
Office of Space Science and Applications
NASA HEADQUARTERS, WASHINGTON, D.C.
and
ASTRIONICS LABORATORY
MARSHALL SPACE FLIGHT CENTER
Huntsville, Alabama

Prepared by
CONVAIR DIVISION OF GENERAL DYNAMICS
San Diego, California

PARABOLIC EXPANDABLE TRUSS ANTENNA EXPERIMENT

INTRODUCTION

The primary purpose of thi s program is to develop an AAP experiment that will demonstrate the feasibility of Large Erectable Antennas in orbit for future communication and navigation systems. The experiment will demonstrate (1) erection of a 100-foot diameter, high-quality antenna for the major frequency ranges; (2) evaluate maximum gain RF patterns — particularly peak sidelobes — and noise temperature; (3) pointing and holding of earth, lower-orbit satellites, and galactic targets; (4) perform transmission tests; and (5) use man's ability to enhance the performance of and simplify a large electro-mechanical system.

Support by the Apollo crew allows the experiment to be performed earlier with greater versatility. Upon CSM departure, a large ground-controlled, refurbishable communication system, with a minimum five-year life, will continue to operate in orbit and be repeatedly interrogated to evaluate its system life.

This volume summarizes the Parabolic Expandable Antenna Experiment. The first part of the study evaluated existing concepts, including inflatables, petals, automated assembly techniques, and several new concepts. At mid-term (Figure 1) a helical array, phased array, and expandable truss paraboloid were selected for study. This work is reported in Volumes I and II of this report.

The third phase selected the expandable truss paraboloid for further development. Its selection was further confirmed in a related program, "Large Space Structure Experiments for AAP," NAS-8-18188, November 1967, in which more than 25 concepts from industry and NASA agencies were evaluated. Selection criteria along with a description of the expandable truss antenna are reported in Volumes I and V of that program, with particular emphasis on man's participation.

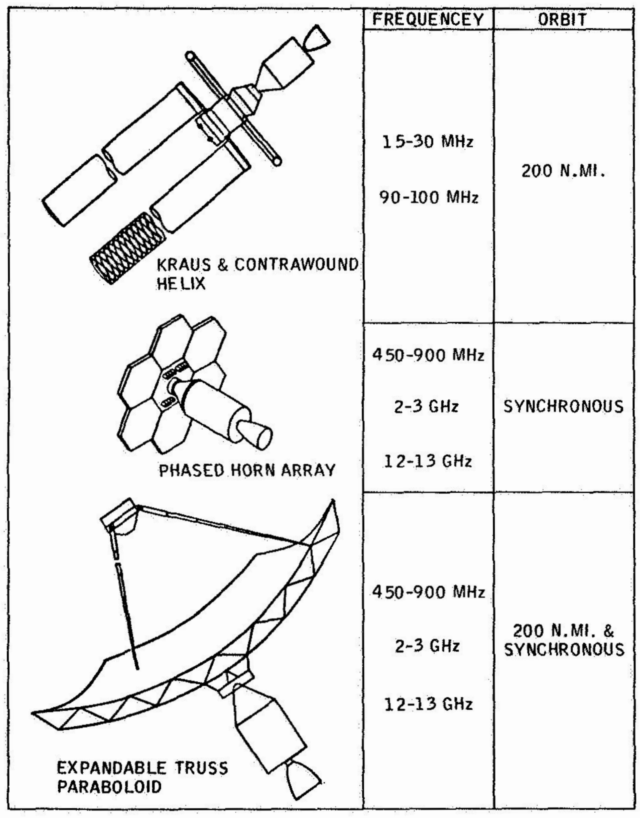

Figure 1

Volume IV of this study presents the Parabolic Expandable Truss Antenna Experiment summarized in this volume and a completed NASA 1347 experiment form.

With the rapid growth of communication systems, large antennas in the 40 to 200-ft. diameter range are required to provide optimum use of an ever-shrinking available frequency spectrum. Large antennas (Figure 2) reduce the beamwidth, controlling the earth reception area of the orbital signal. From synchronous orbit a 17-deg. angle subtends the hemisphere. Two degrees typically covers a 800-mile time zone in the US; at high frequencies a half-power beamwidth of 1/8 deg. would intersect a 50-mile zone.

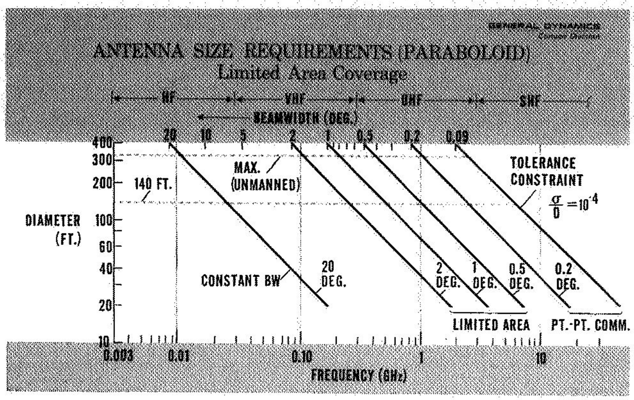

Figure 2

For future orbiting navigation and traffic radar systems, large 200 to 300-ft. ellipsoidal elements of the paraboloid potentially are required to acquire and position moving objects accurately.

Volume in the currently available Saturn fairing would limit the expandable truss antenna size to a 320-ft. diameter in an unmanned launch and to 140 ft. diameter in the LEM adapter area with a manned CSM. A practical reflector tolerance boundary of σ (RMS) to diameter ratio of 10^{-4} limits the efficient useful range of the antenna and the minimum bandwidth.

The Saturn-launched experiment reported in this study would deploy a large 100-ft. parabolic expandable-truss antenna, preferably in synchronous orbit. A 740-sq. ft. omnidirectional solar cell system will provide power for the tests performed in the 100 MHz to 6 GHz range. An expulsion and momentum exchange system is used for station keeping and attitude control. Peripherally mounted telemetry antennas provide continuous data relay to earth. All systems are designed to allow the Apollo crew to improve performance and reliability, and to conduct the test phase of the experiment. Total experiment weight is 5,500 lb., of which the 100-ft. diameter antenna reflector weight of 0.10 lb./sq. ft. of aperture is only a small part. Peak efficient frequency application for the 100-ft. diameter experiment antenna (RMS = 0.125 in.) is 6 GHz, resulting in a 1/8-deg. beamwidth.

A model of the expandable truss antenna with the feed extended and the reflector in the packaged condition is shown in Figure 3. Figure 4 shows the reflector deployed with the Apollo CSM docked to the pressurized feed and electronic compartment. Figure 5 is a photograph of a 7-ft. diameter model with a mesh covering used in RF testing.

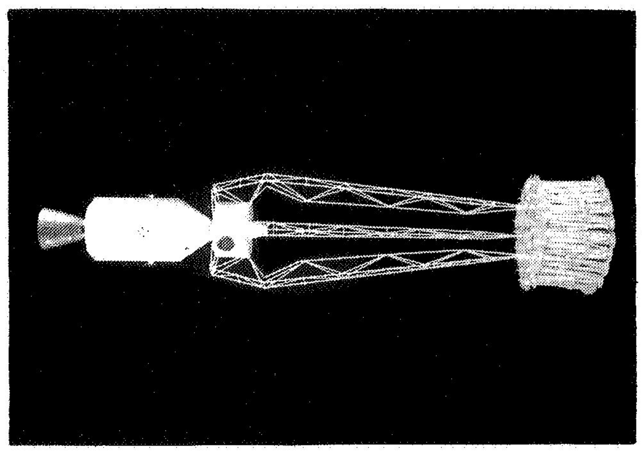

Figure 3

FLIGHT OBJECTIVES

The primary flight objective is to demonstrate the feasibility of a large space erectable antenna. Uniquely, the expandable tubular truss structure can be scaled to many different sizes and shapes. In this experiment, a 100-ft. diameter parabolic reflector and the expandable feed supports form an antenna applicable to many future missions.

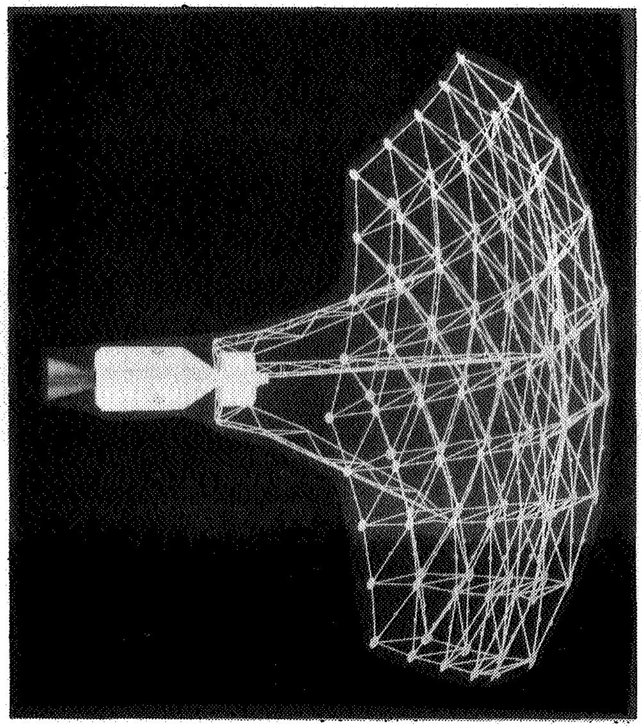

Figure 4

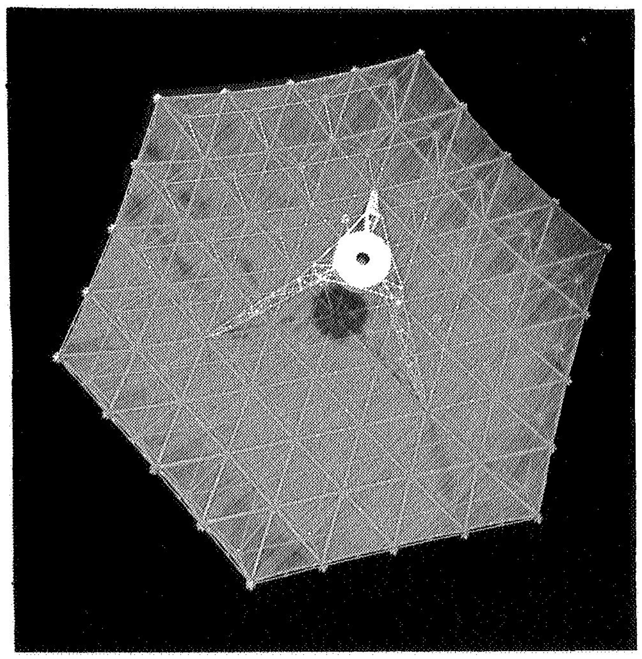

Figure 5

The quality of the erected antenna will be determined from tests of its physical surface, as well as its RF performance. Gain and complete pattern measurements will be evaluated in the 100 MHz to 6 GHz range.

Tests of this kind are not feasible on the ground since a clear sighting of 30 to 50 miles is required. Besides determining antenna efficiency, which significantly affects costly space power systems, extraneous sidelobe patterns that could interfere with transmission in foreign areas are analyzed. Noise temperature measurements will be made at both space and earth orientations.

Narrow-beam transmission tests will be performed at various space and earth environmental conditions to demonstrate the performance of future high data rate links and broadcast systems.

The ability to acquire and hold a target with a large, flexible, narrow-beam antenna is a major problem for both attitude control and structural systems. By acquiring the ground, low-orbit satellites and deep-space probes, this facet of future communication system will be examined. Force field perturbations as they affect large antenna station-keeping and attitude will also be recorded during the life of the systems.

Man's performance is evaluated using biomedical sensors as he participates in a series of orbital tasks. At a console inside the pressurized feed/electronics compartment docked to the CSM, the crew will direct the experiment and monitor subsystems. Typical tasks range from reflector surface measurements, feed boresighting, and RF pattern analysis to acquisition of earth and celestial targets. The compartment is also used as an airlock for EVA tasks.

EVA is required for complete inspection of the antenna, potential repairs, and — most important — adjustment of the reflector mesh for optimum performance. While all structural functions of the antenna are automatic, man can back up every deployment function. Considerable development time and costs are saved by having man available for evaluation, decision-making, and malfunction correction. A summary of the flight objectives is shown in Table 1.

Table 1

	DATA RECORDED FROM	TO RECORD	DURING
1. EVALUATE DEPLOYMENT & STRUCTURAL CHARACTERISTICS	PHOTOGRAPHY STRAIN GAGES ACCELEROMETERS LASTER MEASUREMENT UNIT MICROSWITCHES THERMOCOUPLES	BEHAVIOR OF: EXPANDABLE TRUSS EXPANDABLE FEED MESH REFLECTOR CONTOUR THERMAL VARIATION STRUCTURAL DYNAMICS ANTENNA DEGRADATION	DEPLOYMENT MESH TOLERANCE TESTS PATTERN MEASUREMENTS POINTING TESTS OPERATION EVA SUPPORT
2. RF PATTERN MEASUREMENTS	STAR TRACKERS RECEIVER SIGNAL LEVEL TM & COMMAND SYSTEM STATUS	MAXIMUM GAIN BEAMWIDTH SIDELOBES BACK LOBES	GROUND TRANSMISSION AT 100 MHz, 1 GHz & 6 GHz AT VARIOUS SUN ANGLES & ECLIPSE PERIODS
3. NOISE TEMPERATURE MEASUREMENTS	STAR TRACKERS RADIOMETER TELEMETRY & COMMAND STATUS	NOISE TEMPERATURE OF ANTENNA FOR LUNAR, SOLAR, GALACTIC & EARTH ORIENTATIONS DURING CONTROLLED DRIFT THROUGH TARGETS	
4. POINTING & HOLD CAPABILITY	HORIZON SCANNER SOLAR ASPECT SENSOR STAR TRACKERS RECEIVER SIGNAL	POINTING TOLERANCE HOLD TOLERANCE	WHILE ACQUIRING EARTH TARGETS ORBITING SATELLITES DEEP SPACE TARGET
5. DETERMINE MAN'S CAPABILITY TO SUPPORT A LARGE ELECTRO-MECHANICAL SYSTEM	BIOMEDICAL SENSORS PHOTOGRAPHY	PHYSICAL REACTIONS, DEXTERITY, CAPABILITIES, & TASK ACCOMPLISHMENT TIMES	PHYSICAL LOCOMOTION EQUIPMENT TRANSFER INSPECTION MESH ADJUSTMENT FEED ALIGNMENT TUBULAR ELEMENT LOCKUP
6. NARROW-BEAM TRANSMISSION TESTS	STAR TRACKERS (RECORDED BY GROUND STATION)	SIGNAL STRENGTH SIGNAL/NOISE RATIO PHASE LINEARITY POLARIZATION BANDWIDTH	TRANSMISSION AT 1 GHz & 6 GHz TO VARIOUS POINTS IN U.S. & HAWAII (HIGH & LOW LONGITUDE & NOISE LEVEL) DURING DARK & VARIOUS SUN ANGLES
7. LONG-TERM DEGRADATION OF SYN. ORBIT ELECTRO/MECHANICAL SYSTEM	RF GAIN MEASUREMENTS STRAIN GAGES POWER MEASUREMENT (TM) MICROSWITCHES	STRUCTURAL INTEGRITY MESH CONTOUR POWER LEVEL THERMAL FATIGUE SENSOR POINTING CAPABILITY	

PACKAGING

A major factor in selection of the expandable truss as its packaging versatility. The same size antenna may be packaged in three different enveloped. Figure 6 illustrates the three packaging systems. "A" is a flat "coffee can" package suitable to the LM adapter area; in "B" the top member that hinged inward now hinges outward, reducing the package size but increasing its height; in "C" both external members hinge out, providing the tallest package but the smallest diameter. Typically, a 100-ft. diameter antenna would be packaged in a 15, 10, or 7-ft. diameter package, with the corresponding height 10, 16.7, or 23.6 ft., respectively.

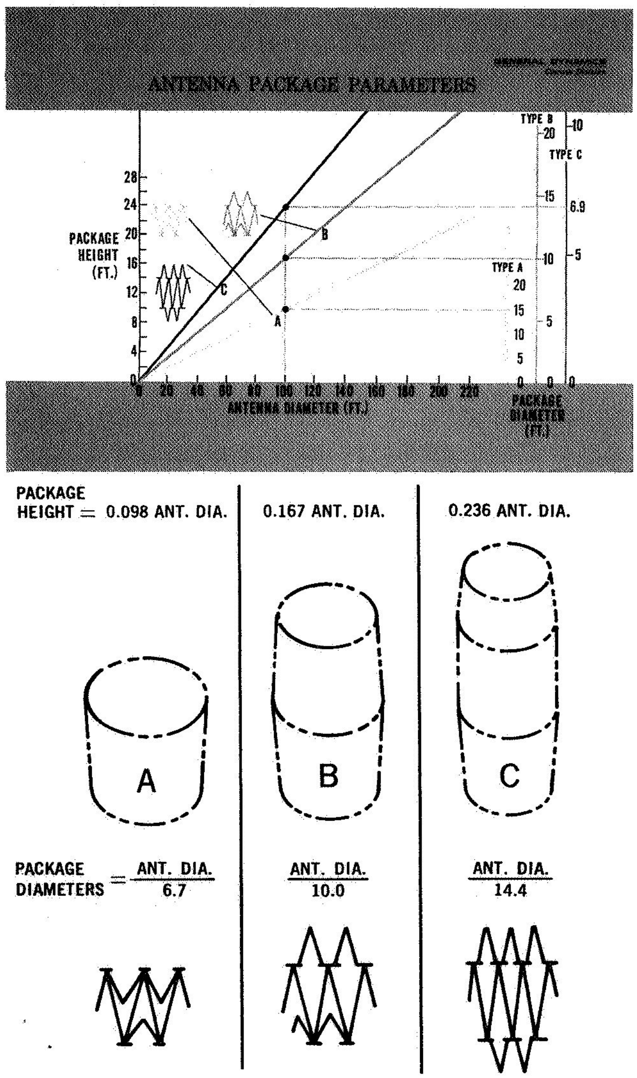

Figure 6

Thus, the antenna developed in this experiment can be conveniently integrated into future systems with different packaging problems. System "A" was chosen for the experiment and is most compatible with the LM adapter area.

The packaged antenna will be supported on a pallet during transportation and during boost (Figure 7). Shear pins at each spider and nine redundant explosive bolts will position the lower spiders on the pallet. The pallet is permanently bolted to four LM hardpoints. A band with dual pyrotechnic release holds the gear-interlocked upper spiders in position until reflector deployment. Four retractable A-frames support the feed and electronic compartment and carry its boost loads directly into the LM hardpoints.

OPERATING SEQUENCE

Figure 8 illustrates the primary operating sequence of the experiment. Boost to synchronous equatorial orbit will take approximately 7-1/2 hours.

Extraction of the antenna experiment is carried out in a manner similar to that of the CSM/LM system, with the exception that the pallet remains with the LM fairing. The crew initiates deployment of the three feed support legs. After checkout to ensure that the feed legs are structurally sound, the reflector will be deployed. IVA and EVA inspection and checkout by the crew will determine if structure and mesh are in position and if all systems are operating.

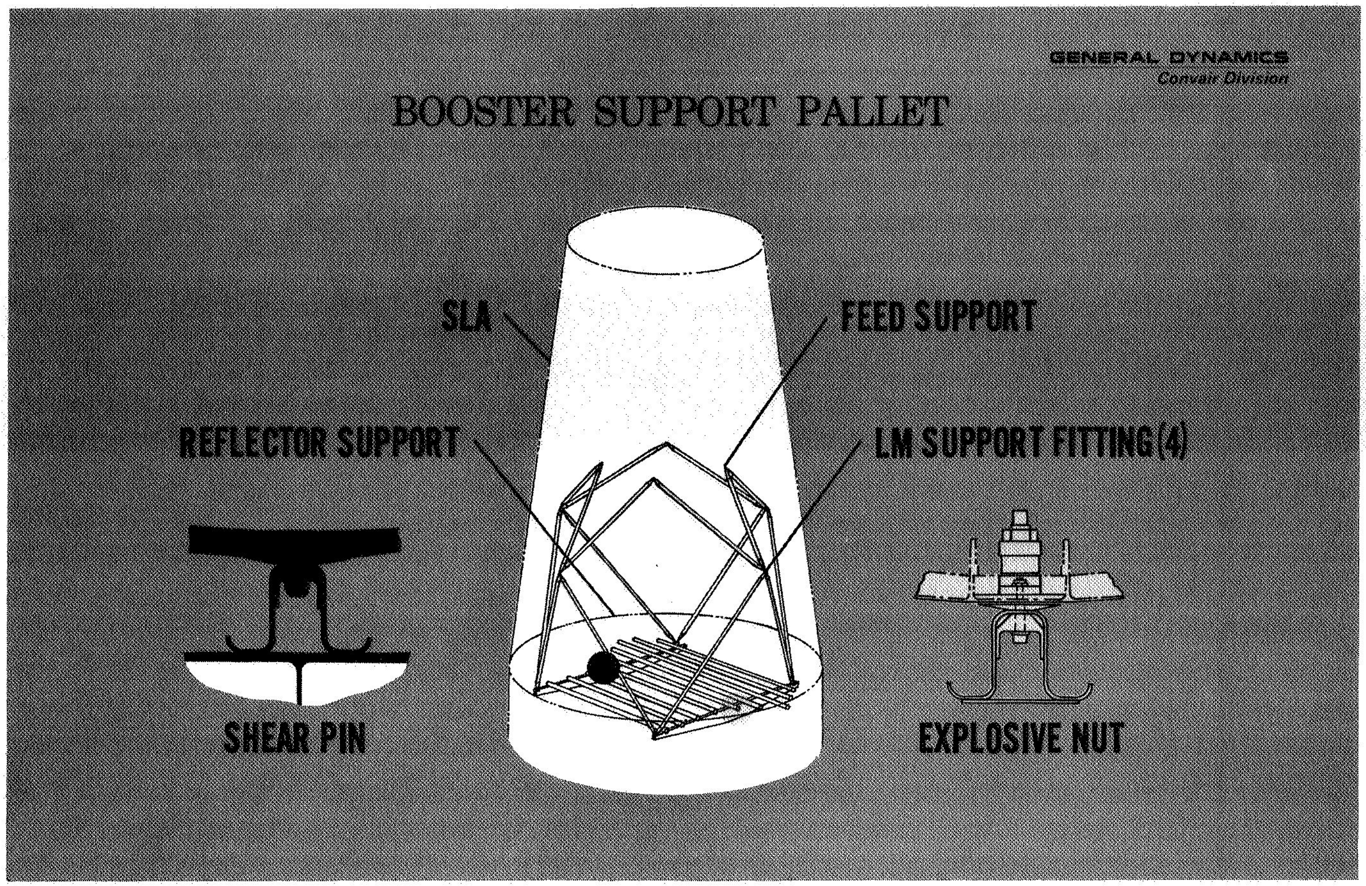

Figure 7

The contour of the mesh surface will be determined with a laser measuring unit capable of scanning the reflector in 30 seconds. Any necessary corrections to the tubular members will be made by the EVA astronaut and the mesh adjusted to optimum performance as required. Tasks and times are listed in Figure 9. Tolerances in the reflector will be biased by moving the feed to the optimum focal point of the best fit paraboloidal surface of the reflector. In addition to determining surface contour, the laser will be used to boresight the feed to the mechanical axis. Pattern, noise temperature, pointing, and transmitter tests will then be made. After a final inspection, the crew will adjust the experiment for automatic operations and stand off to observe its performance.

The antenna will continue to operate in the unmanned mode and will be interrogated periodically as to systems status and maximum gain capability of the antenna. Refurbishment of all systems is feasible to integrate the antenna into an operational system.

The pressurized feed/electronic compartment will contain most of the experiment equipment and receive environmental control from the CSM. Crew activities, planned and abnormal, are listed in Figure 10. Mesh adjustment for improved reflector tolerance is the most likely abnormal EVA task ; a full day is left in the schedule for this activity. Other IVA/EVA tasks could be simulated if the experiment were completely successful: replacing a tubular

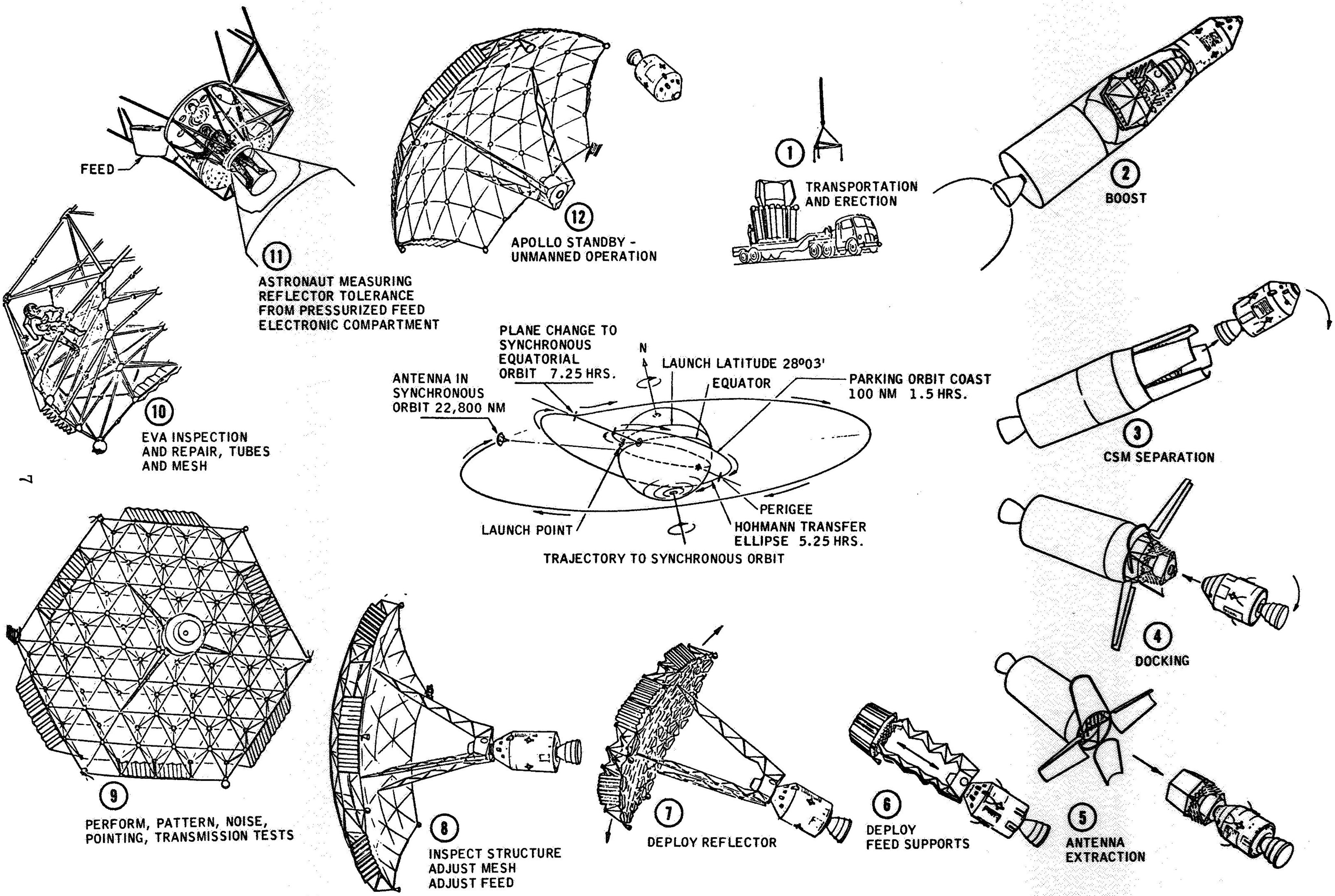
1 TRANSPORTATION AND ERECTION
2 BOOST
3 CSM SEPARATION
4 DOCKING
5 ANTENNA EXTRACTION
6 DEPLOY FEED SUPPORTS
7 DEPLOY REFLECTOR
8 INSPECT STRUCTURE
ADJUST MESH
ADJUST FEED
9 PERFORM, PATTERN, NOISE,
POINTING, TRANSMISSION TESTS
10 EVA INSPECTION
AND REPAIR, TUBES
AND MESH
11 ASTRONAUT MEASURING
REFLECTOR TOLERANCE
FROM PRESSURIZED FEED
ELECTRONIC COMPARTMENT
FEED
12 APOLLO STANDBY -
UNMANNED OPERATION
PLANE CHANGE TO
SYNCHRONOUS
EQUATORIAL
ORBIT 7.25 HRS.
N
LAUNCH LATITUDE 28°03'
PARKING ORBIT COAST
100 NM 1.5 HRS.
EQUATOR
ANTENNA IN
SYNCHRONOUS
ORBIT 22,800 NM
PERIGEE
HOHMANN TRANSFER
ELLIPSE 5.25 HRS.
LAUNCH POINT
TRAJECTORY TO SYNCHRONOUS ORBIT

Figure 8

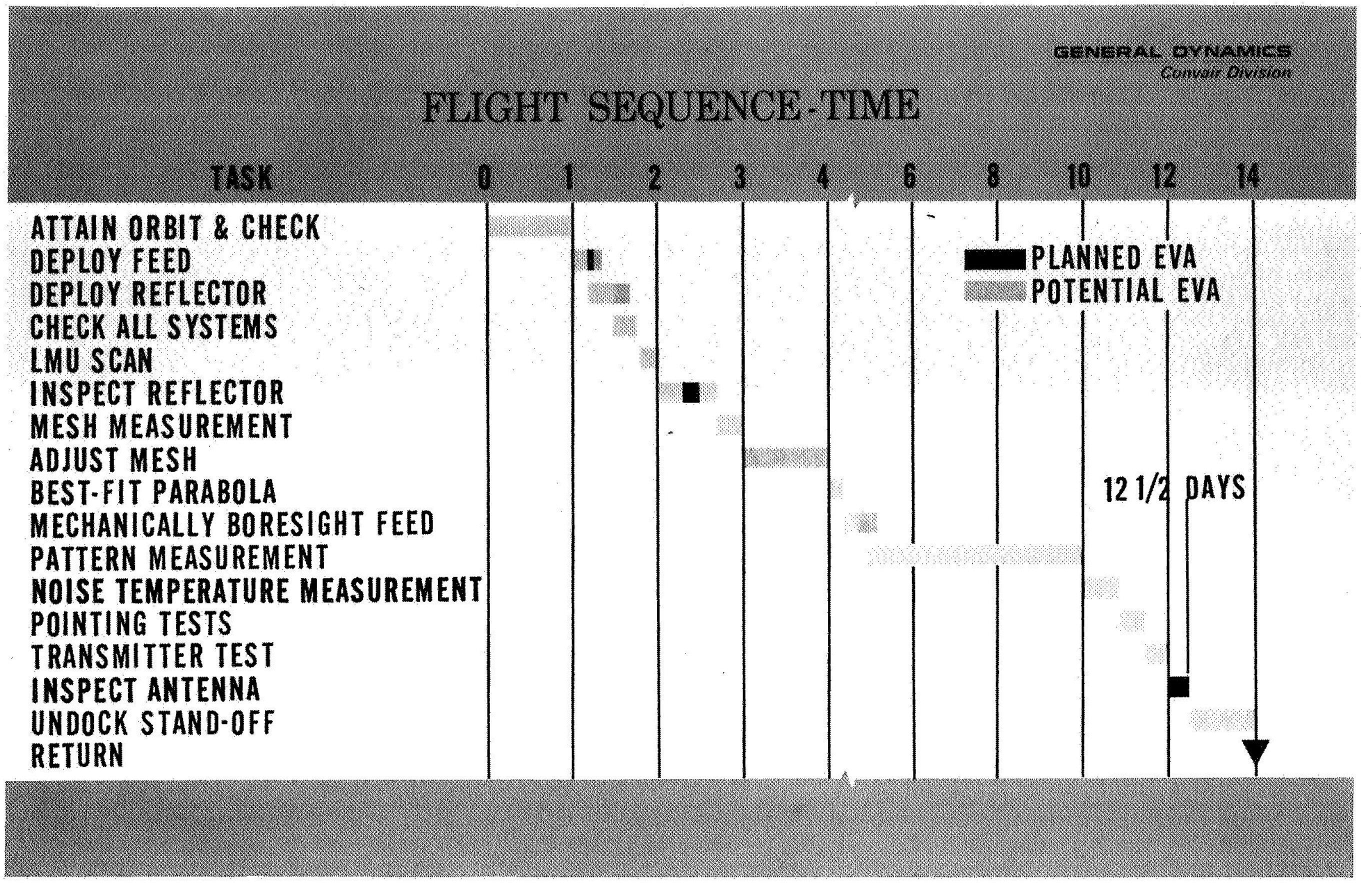

Figure 9

element, splicing or replacing a cable, or manually adjusting the feed. Since every sixth element of the truss is redundant, any one member may be removed without affecting the structural integrity of the antenna. This wide variety of tasks would measure man's ability to support a large electro-mechanical orbital structure.

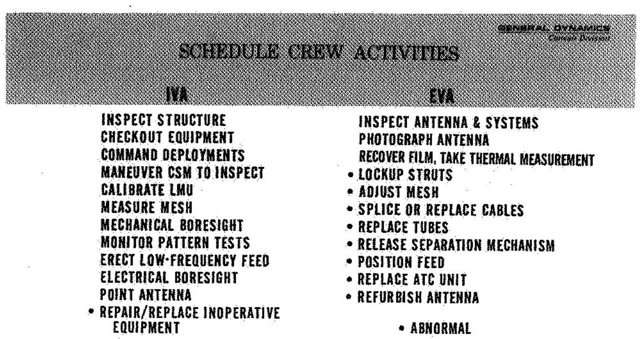

Figure 10

SUBSYSTEMS

Figure 11 shows the orientation of the reflector-mounted subsystems. The natural stiffness and strength of the expandable truss allows a large number of the systems to be mounted directly on the antenna. Dark lines indicate the power, coaxial telemetry, and command system cables. Telemetry antennas are mounted on the periphery for operations when the reflector shadows the CSM from the earth. A three-element highly reliable, cold gas expulsion system may be used for economical gross attitude control and station keeping.

A six-panel, accordion type, expandable solar cell system is integrated into the outer members of the reflector to provide an omnidirectional power system. Three standard gain antennas operating at 100

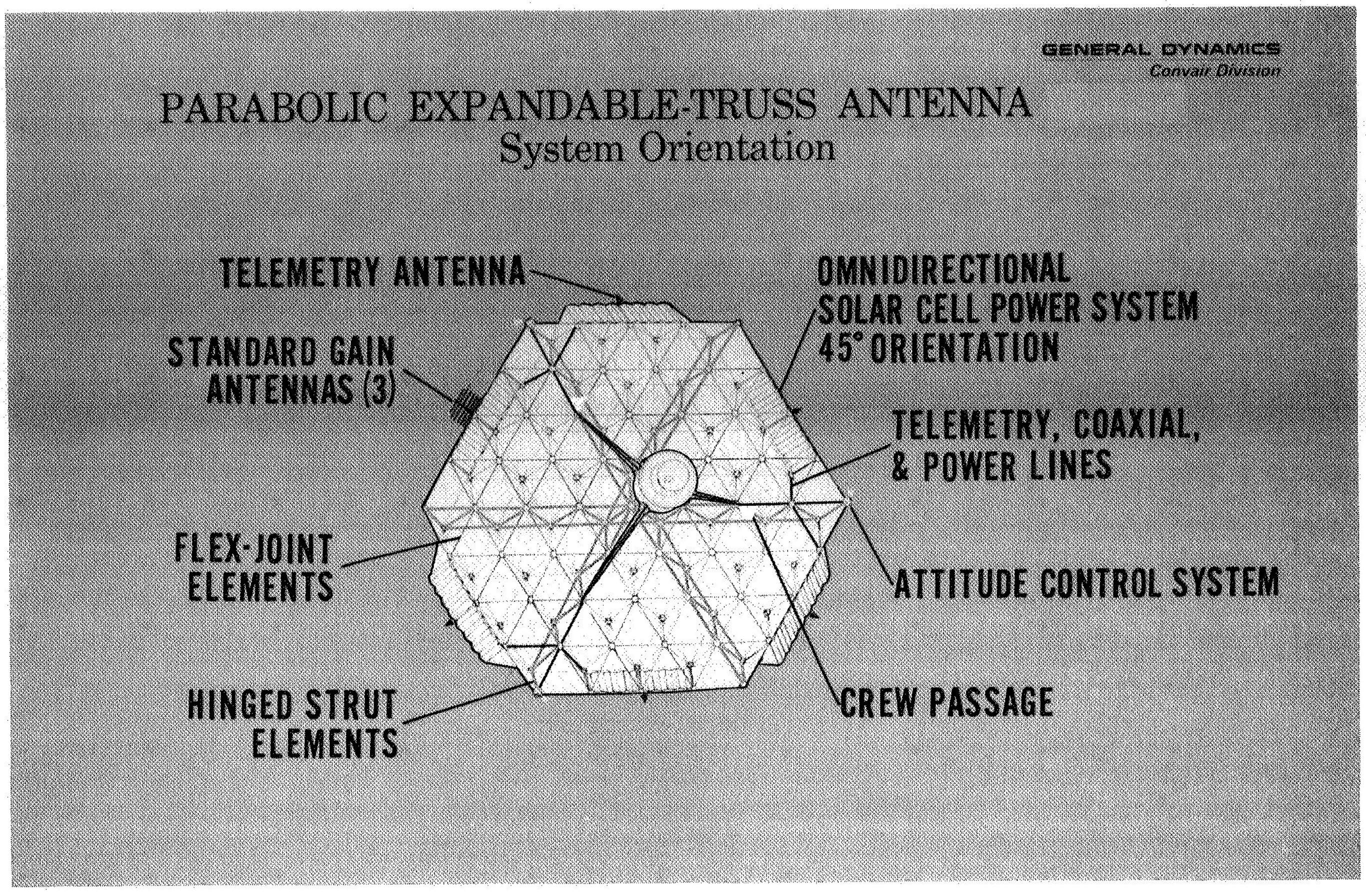

Figure 11

MHz, 1 GHz, and 6 GHz are also mounted along the periphery. Each of the three major diagonals has hinge/lock joints with microswitch instrumentation. The internal joints of these members use the flex (mast) joint for a hinge. Crew passage to the rear side of the antenna is afforded by a triangular hole in the mesh at each feed leg. Communication relay is also provided when the crew is working on the rear side of the reflector mesh. Although the mesh is 80 per cent transparent to light, it will cut radio contact between the EVA man and the CSM.

Structural Subsystem

The expandable truss consists of spring-loaded hinged external and continuous diagonal tubular elements, joining spiders with mesh adjustments, and the flexible mesh system. Deployment of the model truss antenna is illustrated in Figure 12. Figure 13 shows that a beryllium tube would be significantly better on a weight, stiffness, and thermal distortion basis. Perforated aluminum tube is proposed for use in the experimental antenna due to its availability, cost, and the lack of a need for weight saving, as the experiment is presently conceived. The current reflector weighs 0.10 lb./sq.ft. of aperture; beryllium tubing could reduce weight to 0.08 lb./sq.ft. — a saving of 160 lb. on a 100-ft. diameter antenna.

Figure 14 shows three different perforated-aluminum tubular elements (three-inch diameter) that were tested. Tube A proved best, buckling at an average of 1,004 lb.; it weighs 0.013 lb. per foot (B = 714 lb. average, C = 391 lb. average).

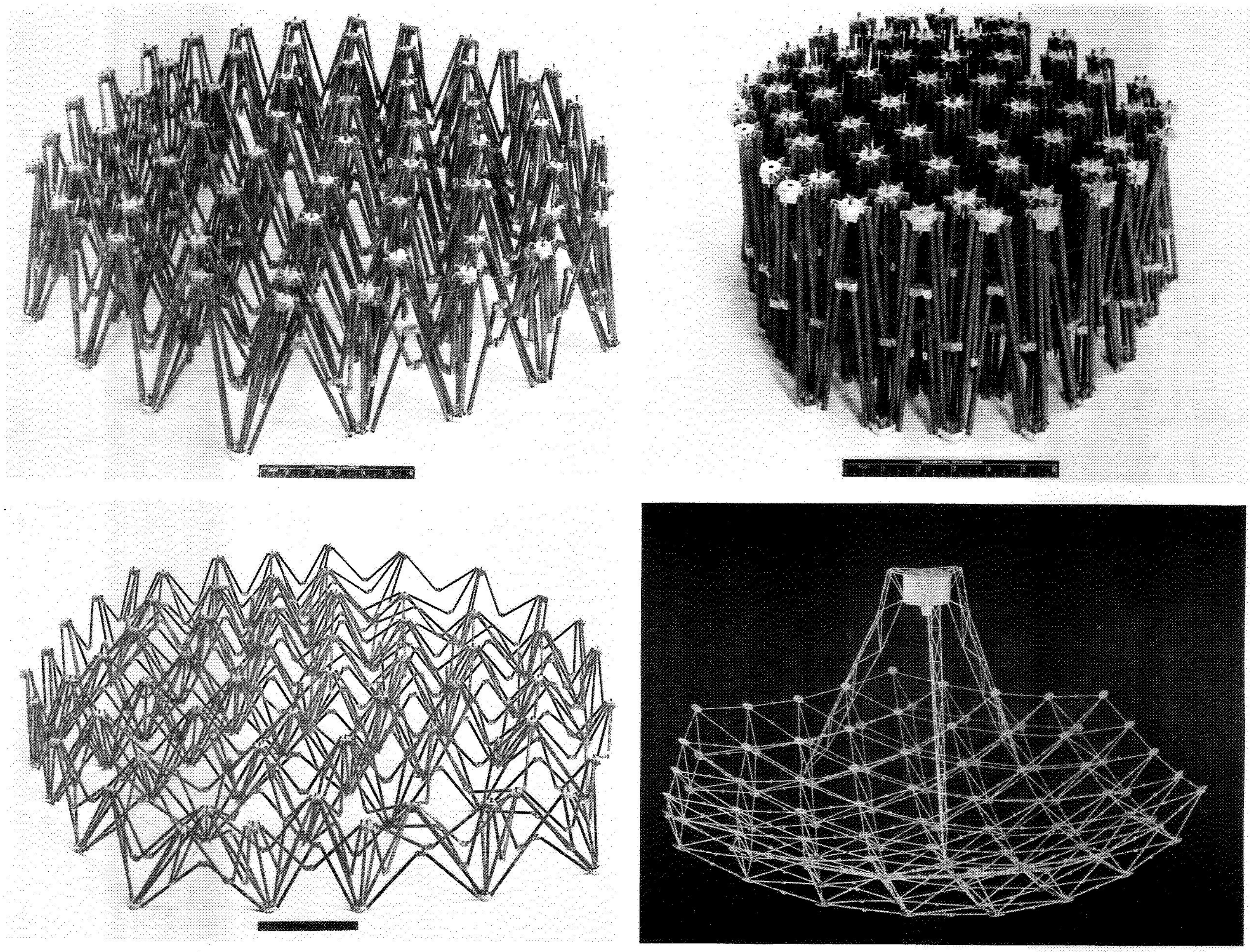

Figure 12. Expandable truss model deployment

GENERAL DYNAMICS

ANTENNA MATERIALS EVALUATION

MATERIAL DESIGNATION	PROPERTY						
	ρ LB/IN.^{3}	E PSI × 10^6	K B/HR-FT.^{2}-°F	α IN./IN.-°F × 10^6	K/α × 10^6 B/HR.-FT^2	MATERIAL INDEX (2)	W/W$_{AL}$ (1)
ALUMINUM ALLOYS							
2024-T4	0.100	10.6	70	12.6	5.55	588	1.000
7075-T6	0.101	10.3	90	12.9	6.97	725	0.775
MAGNESIUM ALLOY							
AZ 31 B-H24	0.064	6.5	56	14	4.0	405	1.056
MAG-THORIUM							
HK 31A-H24	0.065	6.5	61	14	4.35	435	1.411
MAG-LITHIUM							
LA 141-T7	0.049	6.0	25	21.8	1.148	124	3.14
BERYLLIUM	0.067	42.0	87	6.4	13.6	8,520	6.79
LOCKALLOY (BE 38% AL)	0.075	32.0	123	9.2	13.4	5,700	4.02
TITANIUM							
6AL, 4V (ANNEALED)	0.160	16.0	3.8	4.8	0.792	79.2	0.585

(1) MATERIAL WEIGHT INDEX WITH RESPECT TO 2024-T4 AL ALLOY FOR ASTRONAUT IMPACT
(2) MATERIAL INDEX FOR STRENGTH - TEMPERATURE=$(E/\rho)(K/\alpha)$

Figure 13

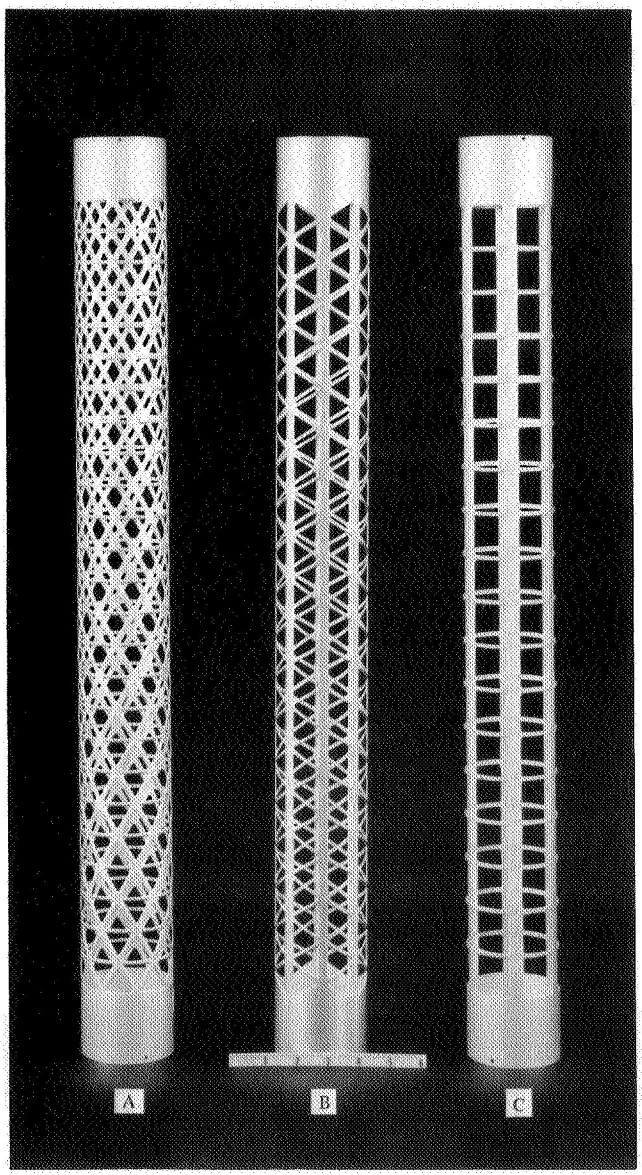

Figure 14. Perforated aluminum truss test sections

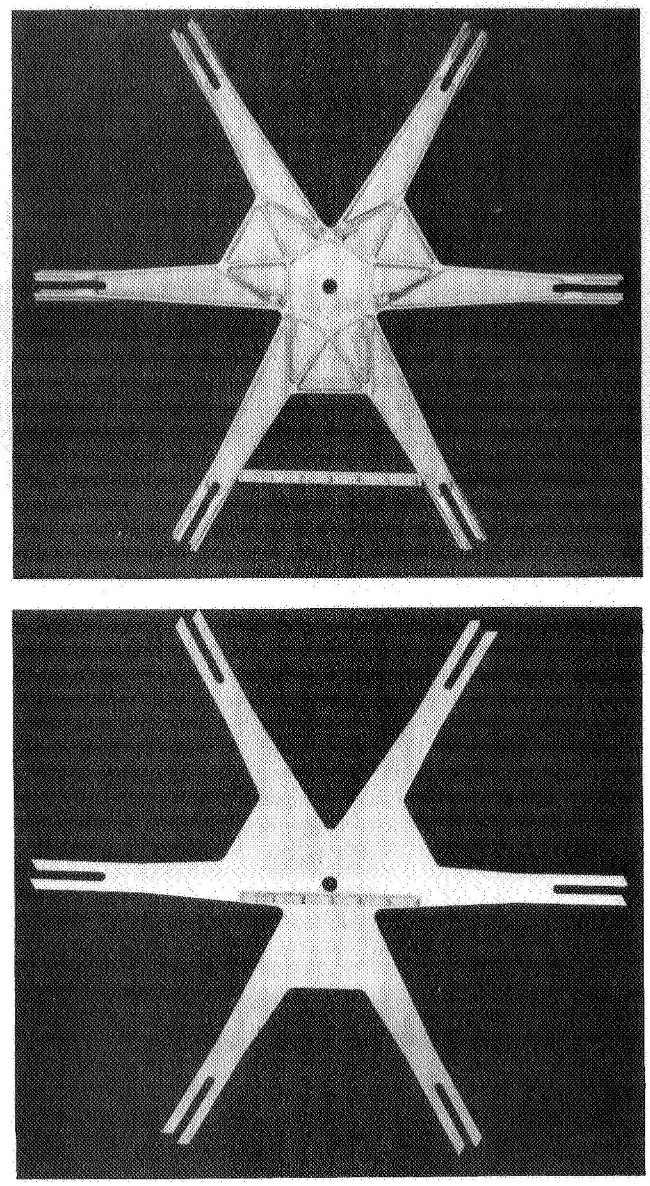

Figure 15. Magnesium spider for 100-ft. diameter reflector

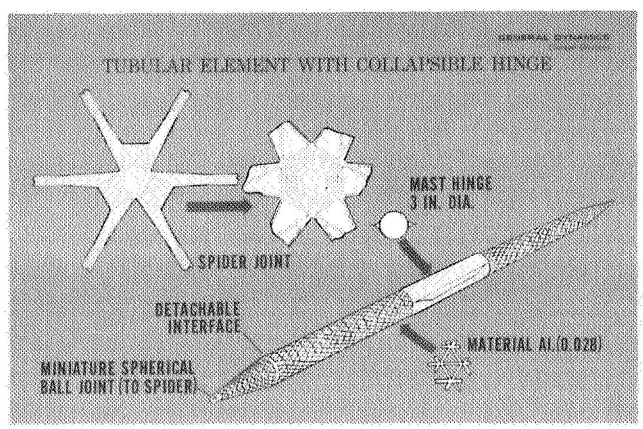

Figure 16

A numerically milled AZ31B magnesium spider for the 100-ft. diameter antenna is shown in Figure 15. Cogged ends of the spider interlock with its six neighbors to form rigid top and bottom elements. Figure 16 shows a typical tube and spider. Twelve mesh adjustment screws are located in the center of the spider. Flexible BeCu hinge joints (Figure 17) are used on all members except the major diagonal discussed earlier. EVA operation during the initial inspection task will ensure that each joint is deployed and locked down (Figure 18).

Reflector Mesh

The critical tolerance element of the antenna is the reflector mesh. Figure 19 illustrates that if the proposed surface RMS tolerance of 0.120 in. for the 100-ft. diameter antenna is doubled, the peak operating frequency would drop from 6 GHz to 3.5 GHz. Half-power beamwidths at the proposed test frequencies are shown for 100 MHz, 1 GHz, and 6 GHz. The deployment sequence of a typical triangular element is shown in Figure 20. Grouped in a fashion similar to parachute material, the gold-coated Chromel-R tricot weave mesh (Figure 21) will feed from flexible retaining rings as the truss elements straighten. RF reflectance of the mesh is -0.2 db less than a solid copper plate at test frequencies up to 15 GHz.

Details of the mesh system can be seen in Figure 22. The white line mesh material is pulled tangentially down to four hexagonal flats in each triangular element by the webbing. Three tension lines (dotted lines) attached to the webbing and the adjustable screw jacks at the spider move the mesh to its best position. This system will be used during ground fabrication and for adjustment by the crew in space if necessary. A summary of the maximum distortion is shown in Table 2.

The key elements in mesh adjustment are the method and accuracy of the measurement system. In this study, a modulated laser system was developed to measure surface contour to ± 0.006 in. The laser unit is mounted at the feed point, 40 ft. above the mesh. A rotating mirror system would allow a complete scan of the reflector within 30 seconds. Mesh reflectance tests indicate that local targets are not needed and that a continuous measurement of the mesh surface contour is possible.

A printout of the surface contour, recommended adjustments, best fit paraboloid surface, and optimum focal point could be provided. Installed at the focal point, on the pressurized feed and electronic compartment (Figure 24), the laser measurement unit, monitored by the crew, would determine the optimum surface contour. Repeated measurements can be made during EVA adjustments (Figure 25). Confirmation of the best-fit focal point can also be determined with the laser. The feed cone will then be swung back over the laser and boresighted through three corner reflectors to match the optimum focal point established by the laser.

Feed-Electronic Compartment

Along with the laser system, the eight-foot diameter pressurized feed/electronic compartment contains the transmitter and receiver, batteries, power conditioning and monitoring equipment, momentum exchange system, and telemetry. With man required to perform, support, or monitor the experi-

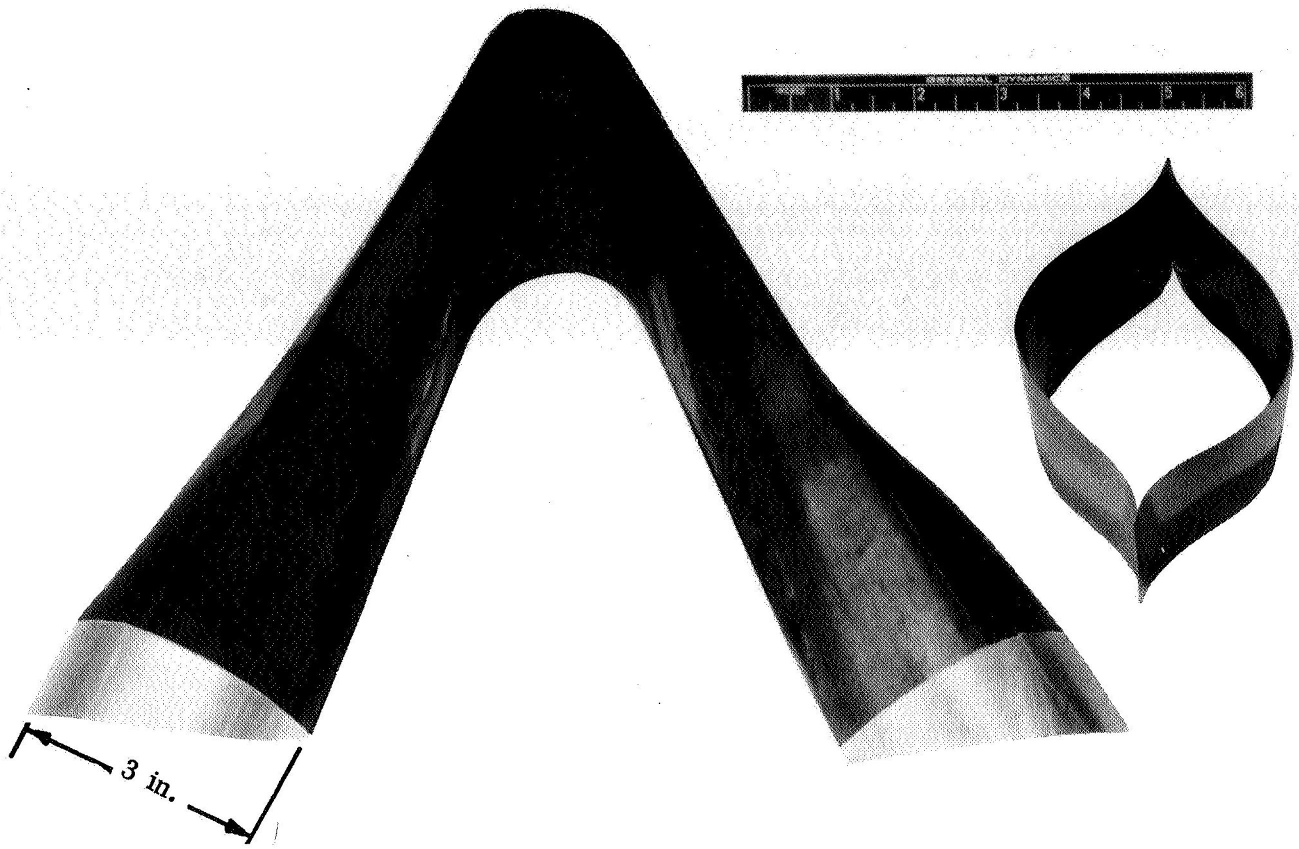

Figure 17. Typical midspan hinge

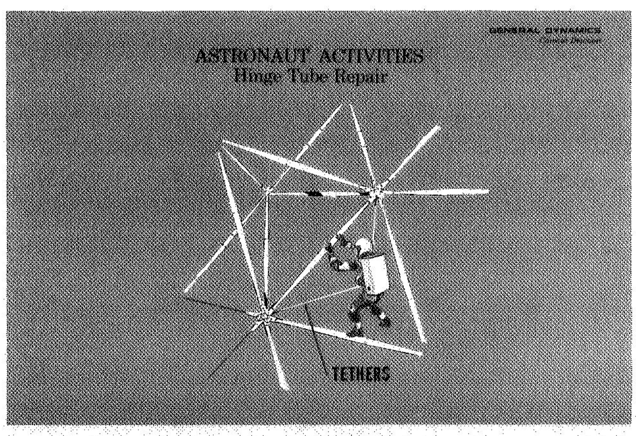

Figure 18

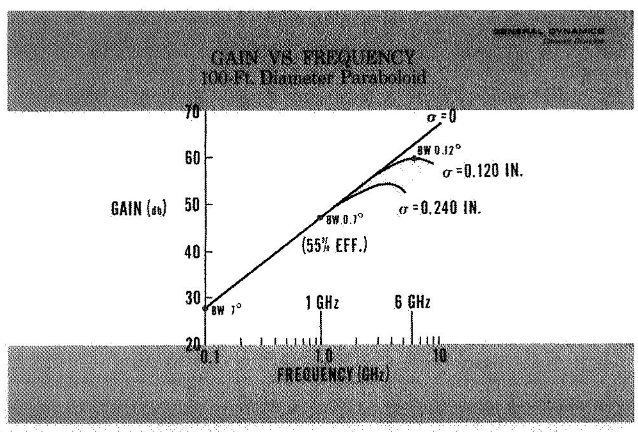

Figure 19

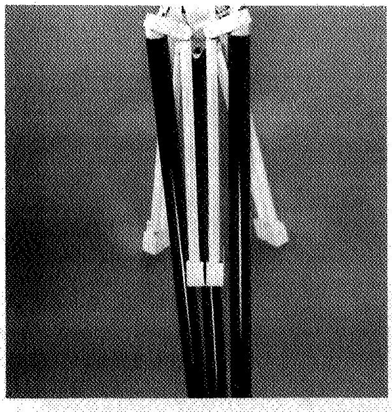

Packaged

Deploying

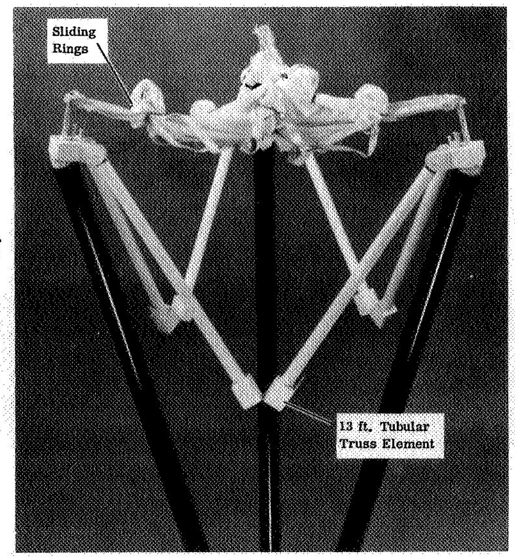

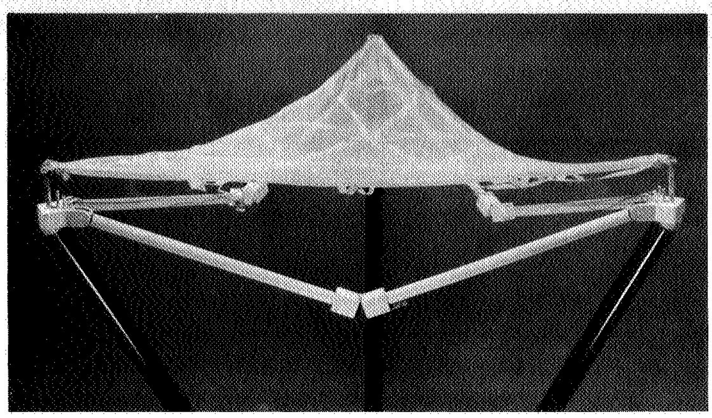

Materials

(1) Tricot Chromel R Mesh
(2) Chromel R Tapes
(3) Steel Cable

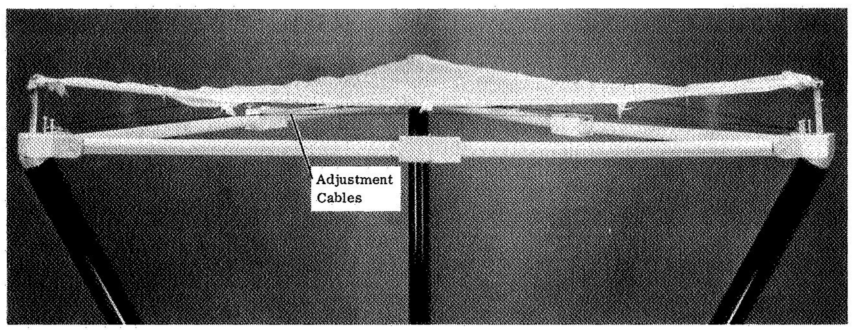

Deploy

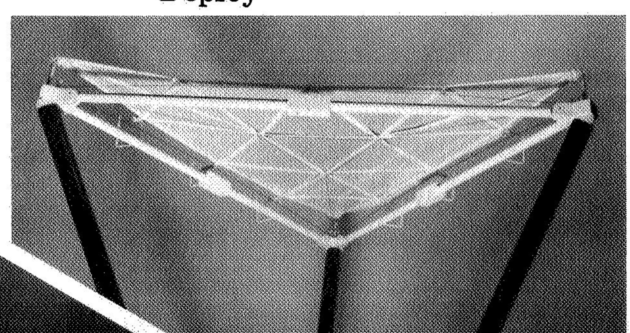

Underside

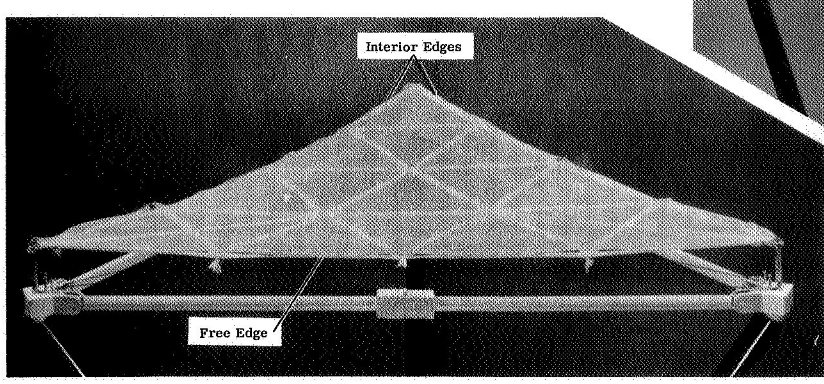

Figure 20

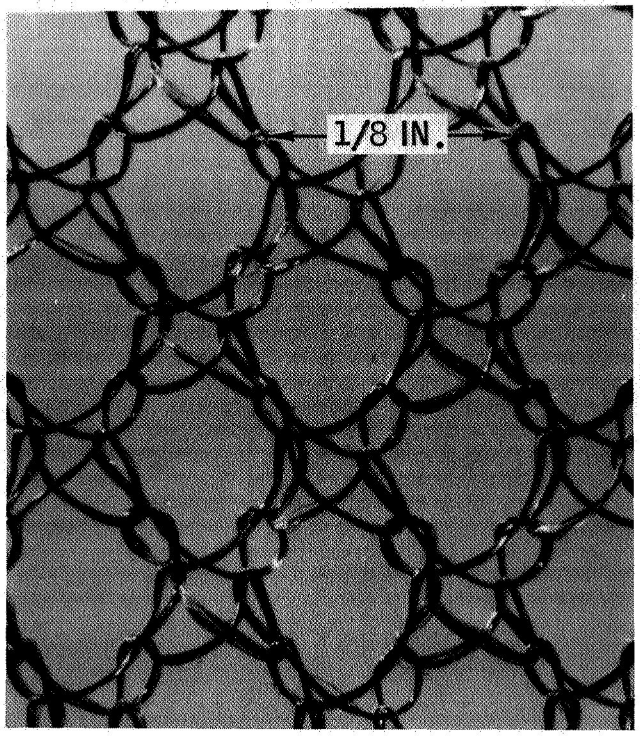

Figure 21. Chromel-R mesh

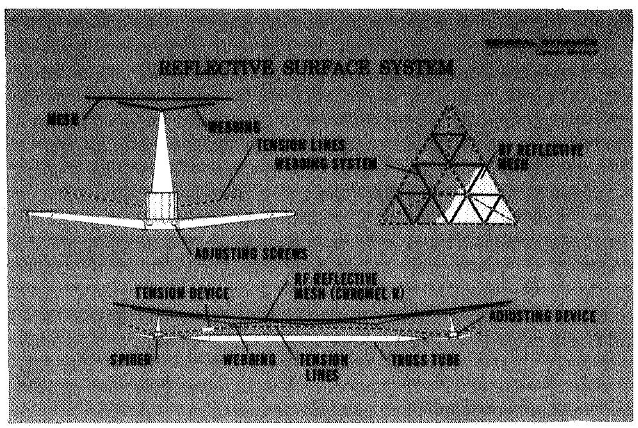

Figure 22

ment over the full 14-day period. a shirt-sleeve environment is required in the compartment. An oxygen pressurization system compatible with the CSM is provided for the compartment, with environmental control supplied by the CSM. Cold plates and external radiators will stabilize the electronic equipment heat load within the Apollo limits. (Figure 26). All equipment must operate in both pressurized and unpressurized environments since the compartment is used as an airlock during EVA tasks.

Table 2

TOOLING LOCATION	± 0.005
BEARING ACCUMULATION	± 0.025
MESH INSTALLATION	± 0.060
MESH CONTOUR	± 0.040
THERMAL (SIDE)	± 0.066
DYNAMIC	± 0.010
MEASUREMENT SYSTEM	± 0.005
	± 0.211

RMS = 0.103 IN.; $\sigma/D = 8.6 \times 10^{-5}$

RECOMMENDED SPECIFICATION RMS = 0.125 IN.

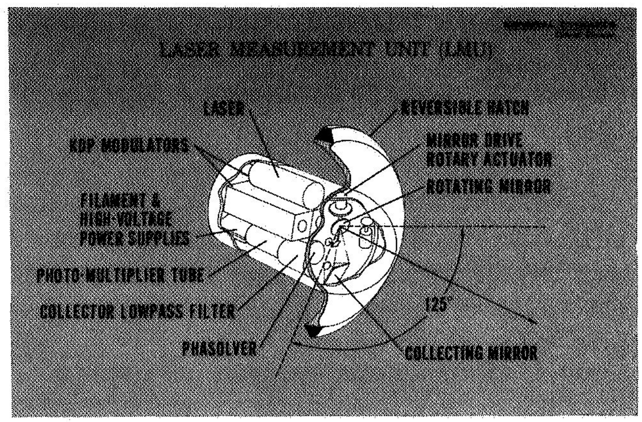

Figure 23

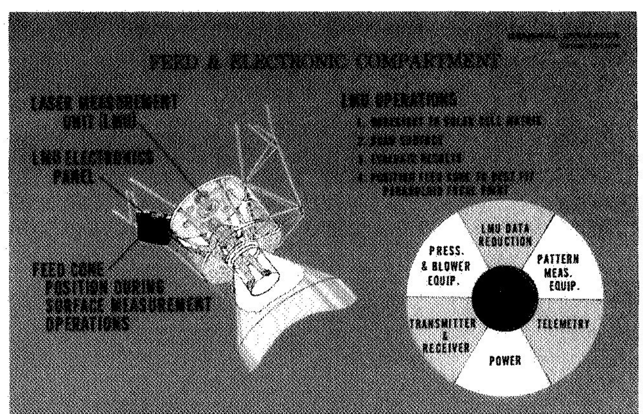

Figure 24

Electrical Power

The power system is a major cost item in the experiment. As the program progesses, every effort should be made to monitor and reduce the power requirements. Figure 27 outlines the basic elements of the system. No development items are anticipated.

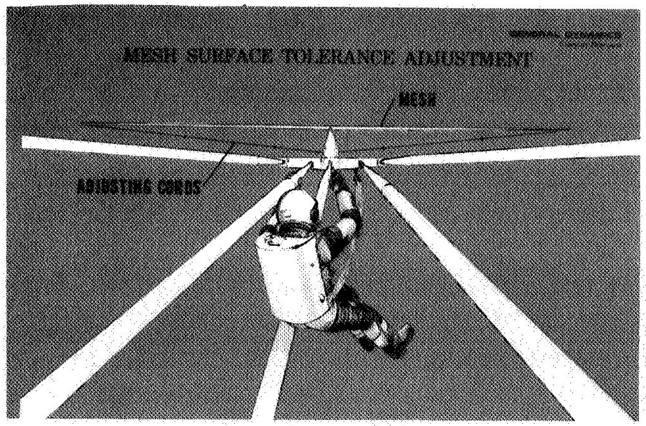

Figure 25

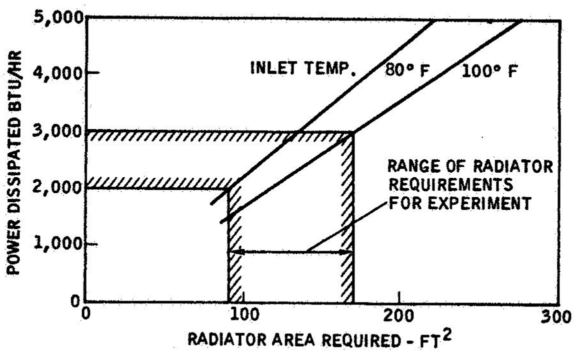

Figure 26

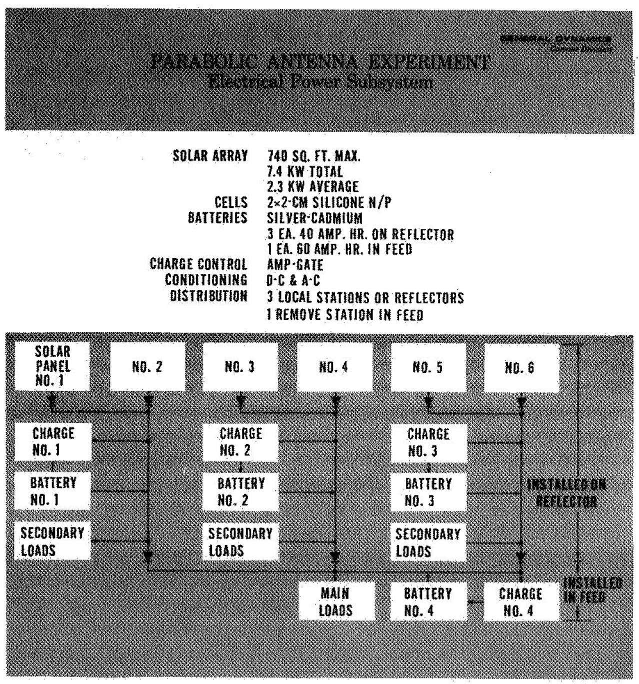

Figure 27

Attitude Control System

To provide the angular rate and attitude control limits required by the experiment in synchronous orbit (Figures 28 and 29), the hybrid control torque system of Figure 30 was configured. A low I_{sp}, but highly reliable, cold gas reaction system is efficient when acting on the long moment arm permissible with the truss antenna. The expulsion system is used for rates down to 0.006 deg./sec. and for station keeping. An inertia wheel system is used for correction from 0.66 to 0.001 deg./sec. A synchronous orbit, two-year life system requires 200 lb. of propellant with 70 lb. assigned to station keeping.

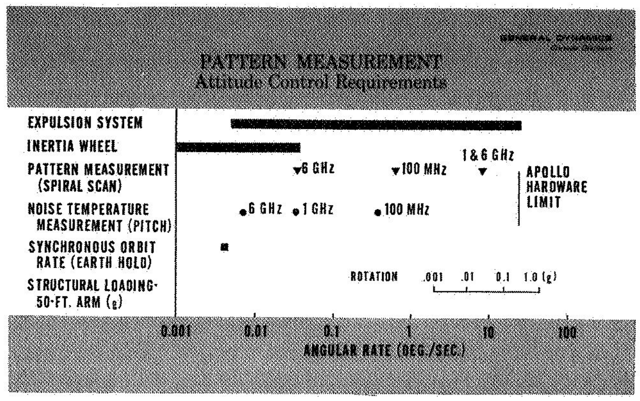

Figure 28

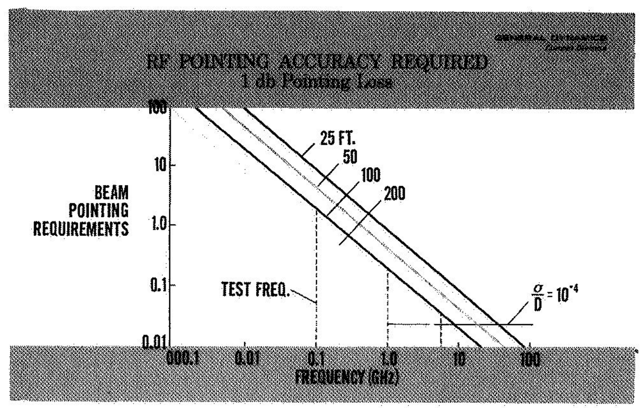

Figure 29

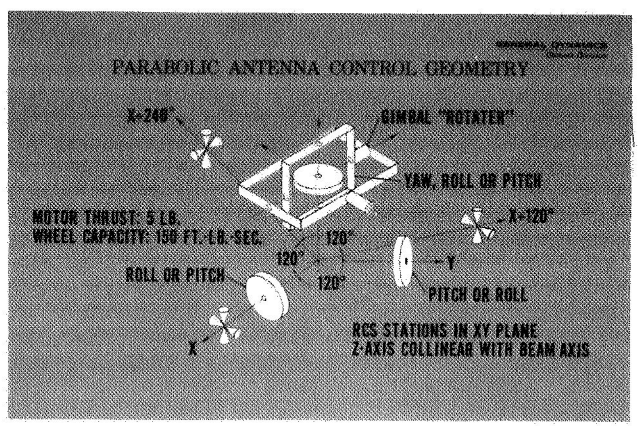

Figure 30

The inertia wheel system has several redundant features in that the yaw wheel can be operated in a control moment gyro mode to generate a spiral scan efficiently. In the instance of a pitch or roll wheel failure, the less critical yaw axis can fall back on reaction control and loan its wheel to the failed axis.

The star tracker system illustrated in Figure 31 provides the desired sensor accuracy and references all pointing to the inertial reference of the star field. A horizon scanner and a solar aspect seeker will determine the basic reference with the star tracker providing the fine control. Precision in torque control and attitude sensing can be seriously degraded if the elastic properties of the working platform make the star tracker, in effect, the analog of a micrometer on the end of an oscillating yardstick. Figures 32 and 33 effectively point up the nature of the deterioriation in the ability to hold attitude, as a function of a change in natural frequency (or stiffness) of the antenna structure and the degree of compensation for structural feedback through the star trackers. Figure 32 isolates the vibratory contributions to beam motion and emphasizes the necessity of a relatively rigid structure and care in the selection of sensor location or compensation, if accurate pointing is to be achieved. Figure 33 illustrates the considerable gain in pointing accuracy potential when a compensated inertia wheel system is used. It is evident in this figure that the principal limitation lies with the sensors. The rigid expandable truss has a natural frequency of 2.8 cps for the reflector and 1.6 cps (10 rad./sec.) for the combined feed-boom structure. A computer-aided analysis has been used to determine the basic modes of the reflector.

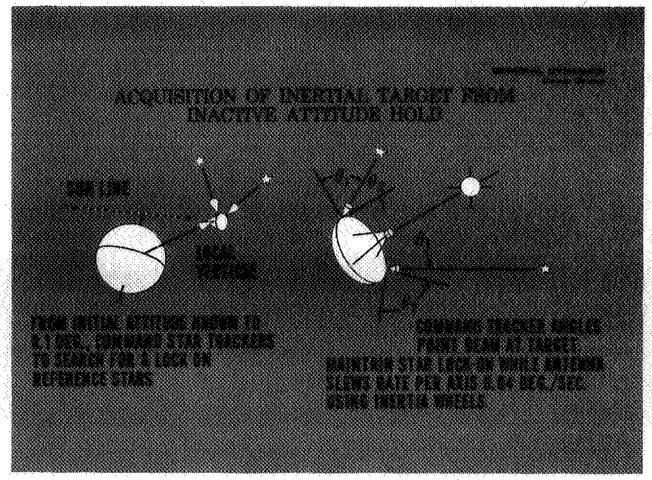

Figure 31

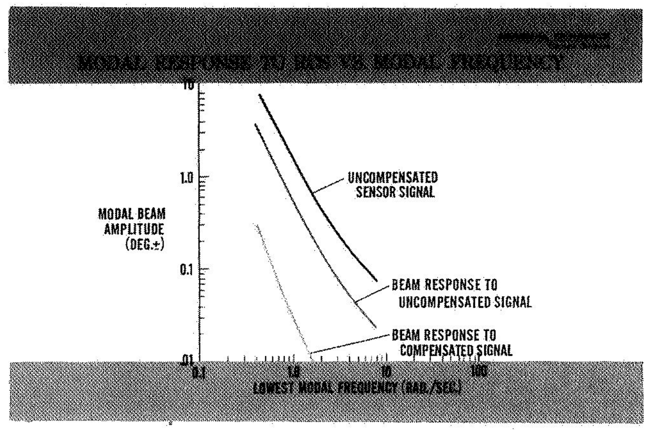

Figure 32

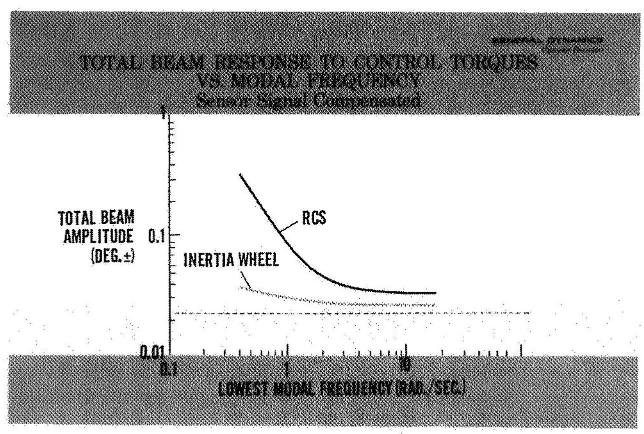

Figure 33

This ultimate dependence on structural stiffness can be met by the truss type parabolic antenna because of its inherent stiffness and the relative ease with which the stiffness can be increased to levels commensurate with the extremes of pointing accuracy envisioned for this experiment and the future system.

Telemetry and Command

The design of the telemetry and command system is based primarily on the requirements and constraints of performing unmanned measurements intermittently for a one to five-year period, preceded by an initial 14 days of manned operation. Data collected from the various measurements in the experiment will be channeled to the USB transponder for transmission to earth.

Two telemetry antenna systems will be available: high gain or omnidirectional. The space erectable antenna (52 db) can be used for a high rate data link when not used in pattern and gain measurement tests.

The command system is required so that a number of vehicle functions may be initiated from the ground and to transmit digital data to the spacecraft. Functional commands are associated with deployment of the experiment and to control antenna position, data storage, and transmission. Figure 34 is the basic block diagram of

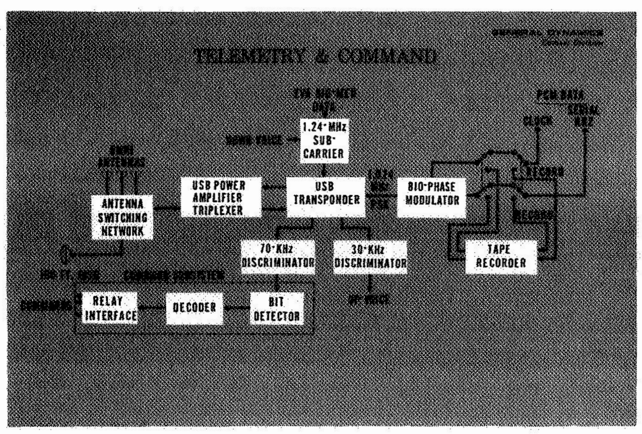

Figure 34

the system. The system will use the available Apollo equipment; no new development areas are anticipated.

Experiment Data Conditioning

Along with the RF parameters, mechanical, thermal, and surface measurement data will be collected for antenna evaluation (Figure 35).

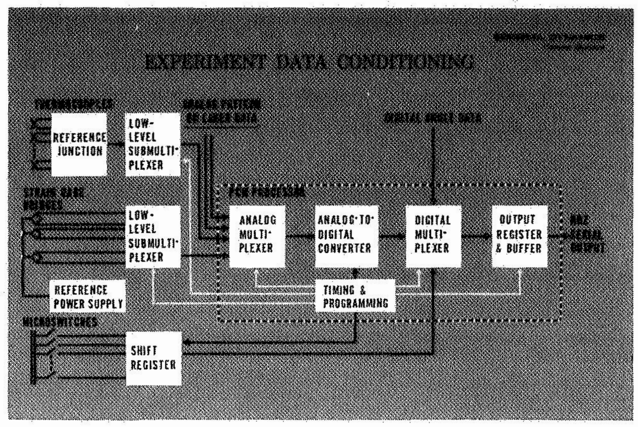

Figure 35

Thermocouples will be located at key positions on the surface of the antenna to evaluate thermal gradients. Strain measurements will be instrumented in near locations to correlate mechanical distortion and stresses with thermal gradients. Microswitches will monitor the lockup of the hinged joints in the antenna structure. The status of the switch contacts will be scanned and transmitted via the PCM telemetry system. The laser measuring unit, used to provide data for surface contour evaluation, produces an analog signal corresponding to distance or range and two digital signals corresponding to angles. This data will define the antenna surface shape. A similar set of measurements is required for the pattern test discussed later.

Maximum bit rates for this experiment are one-fourth the current Apollo LOWAR rate of 51.2 kilbits per second.

PATTERN MEASUREMENT

Radiation pattern and absolute gain define the basic characteristics of an antenna. Pattern measurement consists of determining the relative antenna radiation intensity and the direction at which the intensity occurs. Two orthogonal polarization components of relative power density or electric field intensity, and two corresponding angles in orthogonal components, are measured at each pattern point to describe the pattern completely. Figure 36 shows the basic field intensity measuring and recording system for the test.

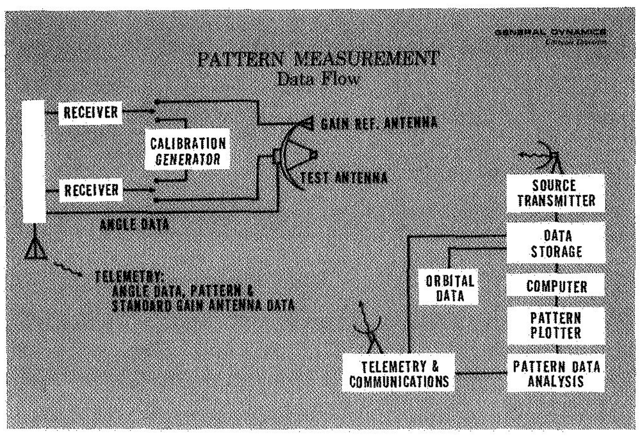

Figure 36

In the proposed measurement, patterns of both space-erectable and standard gain antennas are mapped simultaneously to determine the two pattern peaks. Both receiving systems are calibrated from a common signal generator so that the differential effects of transmission line components and receiver operation can be accounted for in calculations of the absolute gain.

Orbit and Source Selection

Pattern measurements with large antennas having corresponding small beamwidths are best performed in synchronous orbit. In synchronous orbit, there is continuous ground source visibility, data transfer and processing is facilitated, orbital motion can be used for one pattern coordinate angular change, orbital rates are sufficiently low to allow use of low-torque auxiliary attitude control units, and steering maneuvers are simplified. Further, the antenna is evaluated in the most likely operational orbit of a future system.

Severe measurement limitations are encountered in the low orbit configurations when attempting to use a ground source. Operational time is limited to approximately 20 minutes per day (two consecutive passes in a 24-hour period with 10 minutes over target). Within these time constraints, only limited pattern measurements can be conducted, generating approximately 70 per cent of the significant data required for complete evaluation of antenna performance.

Of the various radiating sources considered, Figure 37, (earth-based, stellar, RF satellite, lunar-based), a ground station was selected because of the advantages of experiment flexibility, polarization and radiated power control, frequency control, extensive instrumentation facilities, environmental control, and easy maintenance.

If the experiment is forced to a lower orbit (300 miles) by booster cost, availability, or other operational constraints, testing is best accomplished with an RF satellite source deployed from the parent spacecraft (Figure 38). Although more costly in terms of special instrumentation and satellite deployment complexity, it is preferred over the low-orbit/ground-source configuration because of continuous source visibility, greater quantity of recorded data, and efficient utilization of experiment time.

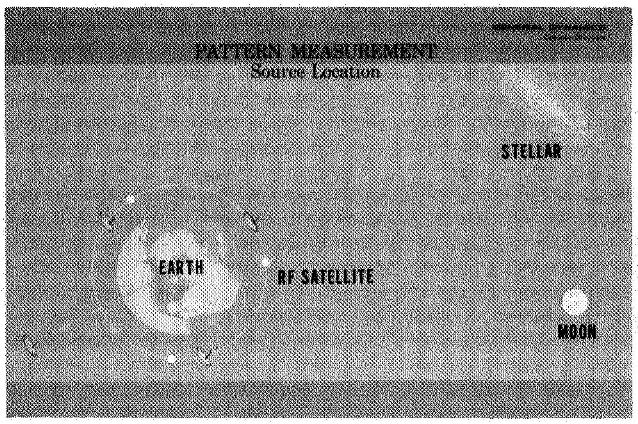

Figure 37

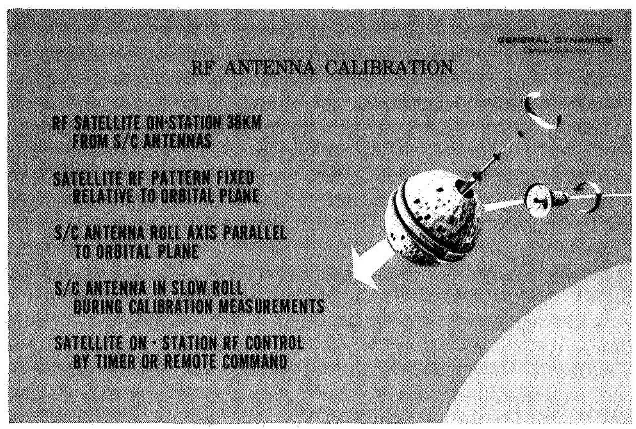

Figure 38

In a fourteen-day experiment, 30 per cent less data would be obtained at a 300 n. mi. orbit compared to a synchronous orbit. With a high C_D A/W, the antenna orbit will decay in 60 to 90 days, depending on orientation, without orbit maintenance; ΔV requirements, would require the attitude control system to change from a cold-gas system to a storable, high I_{sp} propellant.

Transmitter Power Requirements

Figure 39 shows the ground transmitting source output power requirements for measuring the 100-ft. parabolic antenna as a function of frequency for three common sizes of ground antennas in current use (30, 60, and 85-ft. diameters). Assumptions are -100 dbm reciever sensitivity, 2 db system losses, and a 40-db dynamic range for pattern recording. Since the satellite, at the 120-deg. longitude neutral stable point, would be within view of the JPL Goldstone facility, the power requirements with a 210-ft. diameter ground antenna are also presented in Figure 39. None of the power requirements shown is difficult to achieve if the transmitters are located on the ground; any of these antennas could be used with suitable feed modifications to accommodate the test frequencies.

GROUND POWER REQUIRED
FOR PATTERN TESTS

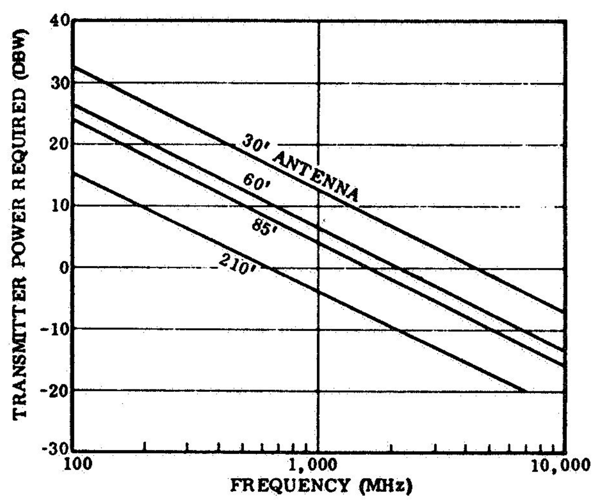

Figure 39

Pattern Scanning Maneuvers

Considering the restrictions of mission time, data rates, hardware cost, propellant, and reaction control engine life, the most promising scanning techniques for space application are great circle and spiral scans (Figure 40).

The conical cut cannot be taken in space because of orbital motion. Scanning by a raster motion is eliminated by excessive fuel requirements. A potential variation of the raster scan, which conserves propellant, is a nodding or oscillating scan generated by a soft spring interconnection between a large mass (such as the CSM) and test antenna. The system becomes a mechanical oscillator when excited, developing a sinusoidal trace over the radiation sphere.

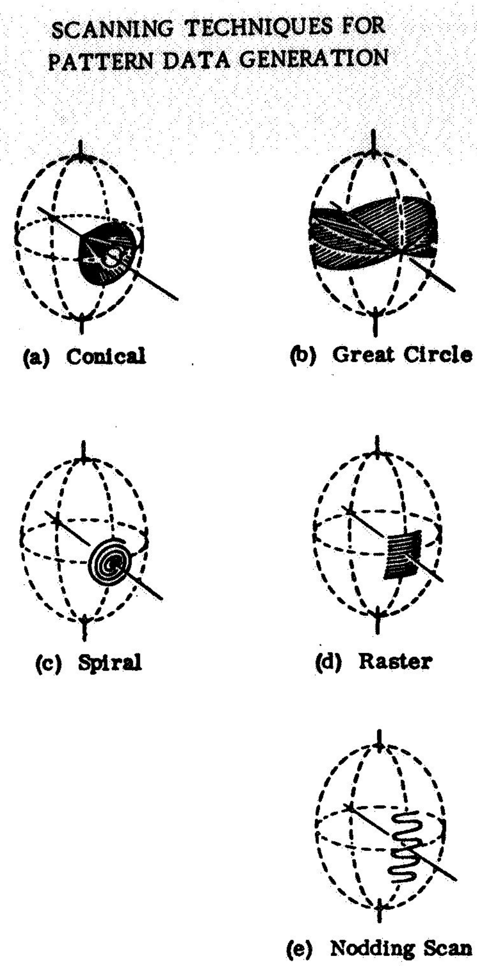

Figure 40

Angular changes for pattern recordings are generated by two effects: orbital motion, and spacecraft attitude changes induced by control devices. An independent attitude control system is designed into the antenna experiment using cold-gas engines and an inertia wheel system. The angular momentum units are effective attitude control devices for pattern mapping at synchronous altitudes where steering rates are small. They are used in this experiment to generate a fine spiral trace about the antenna axis (± 1.5 deg.) for boresighting, focusing, and gathering detailed mainlobe and sidelobe data. Combinations of RCS-induced spin rates and orbital motion are used to generate a more coarse spiral trace over the radiation sphere. Angular momentum units are also used for most of the noise temperature measurements to create the slow angular drift rates required.

Noise Temperature Measurements

Noise temperature measurements require more sensitive instrumentation than the pattern measurements, but are less taxing on the spacecraft attitude control system and measurement bit rate since slow drift rates and small sampling rates are involved. Figure 41 illustrates the noise temperature measurement system.

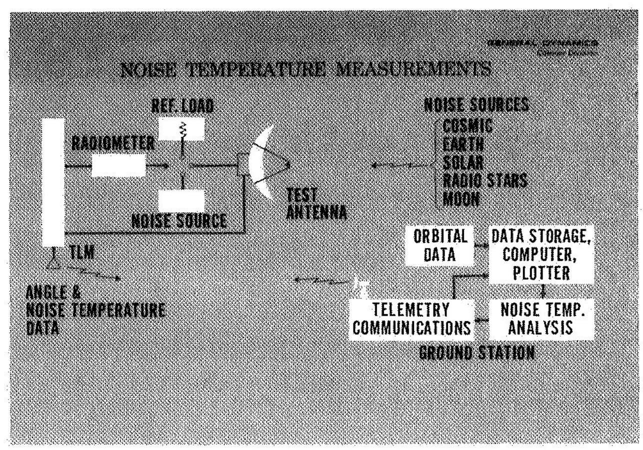

Figure 41

Bit Rate and Significant Data Time

It is apparent that certain regions of the antenna radiation pattern have greater significance in RF performance evaluation. Detailed pattern measurements over the main lobe and near-in sidelobes will define the major portion of antenna characteristics. Since this is a small portion of the radiation sphere, mapping can be accomplished in a relatively short time. Second in importance is the remaining portion of the pattern containing wide-angle sidelobe, backlobe, and reference pattern data for long-term antenna degradation analysis. This data, however, takes considerable time to record in detailed sampling increments. Least in importance, but again requiring a large experiment time increment, is the cross-polarized pattern component. The partial directivity contribution from this component can be obtained, with a fair degree of accuracy, from a scale model test.

Continuous measurement time required to complete a spiral scan over these regions is shown in Figure 42 for the 100-ft. parabolic antenna at synchronous altitude.

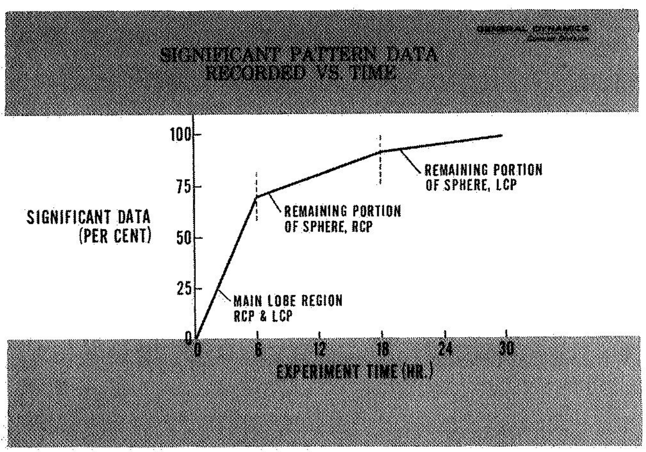

Figure 42

Peak bit rate occurs when 1 and 6 GHz tests are performed simultaneously. Table 3 outlines the measurements.

Astronaut Participation - RF Measurements

Presence of the astronaut simplifies antenna measurement procedures, eliminates redundant equipment requirements, and enhances measurement reliability. His participation in pattern measurement experimental activity includes:

Table 3

PATTERN AND GAIN MEASUREMENT BIT RATE (ONE RPM ROTATIONAL RATE)

MEASUREMENT	TOTAL BITS	SAMPLING RATE (SAMP./SEC.)	BIT RATE (B/S)
TWO ANGLES	28	150	4,200
TWO AMPLITUDES (1 GHz)	14	34	476
TWO AMPLITUDES (6 GHz)	14	150	2,100
TIME			240
SIMULTANEOUS MEASUREMENT BIT RATE, 1 AND 6 GHz			7,016
MEASUREMENT BIT RATE, 6 GHz ONLY			6,540

1. Calibrating electronic equipment by functional switches, amplitude control, and visual observation.
2. Aligning and periodically updating the inertial measuring unit from celestial observations.
3. RF instrumentation checkout and spare unit installation.
4. Manual feed deployment if automated mechanism fails.
5. Making final feed adjustments, based on boresight pattern data.
6. Monitoring data and logging comments during the experiment.
7. Boresighting optical trackers to mechanical pointing axis.
8. Maneuvering spacecraft to point at stationary and earth-based targets.
9. Aligning pointing axis to initial scan position and realigning periodically as discrete angular pattern sectors are covered.
10. Initiating and stopping scanning motions.

11. Aiding target acquisition by monitoring amplitude of detected RF signals and by making visual observations.

12. Initiating alternative measurement procedures if failures occur.

13. Making final equipment checks and connections for unmanned mode of operation.

RF Model Test

In the latter portion of the contract, RF pattern and gain measurements were conducted on a model of the expandable truss antenna. A silver-coated nylon mesh reflecting surface was installed on the truss structure by means of a backup webbing attached to a series of standoffs at each spider connecting joint (See Figure 43).

Stand-offs were adjusted to allow the mesh to best fit a template contour cut for a focal length to diameter ratio of 0.4. No further adjustments of the stand-offs were made for the initial RF measurement results shown in this report.

Measurements of beam pattern and absolute gain were made from S-band to K-band as funding allowed. A typical antenna pattern taken at 7.5 GHz is shown in Figure 44. Sidelobe levels improved at lower test frequencies (-23 db at 4 GHz) and were degraded at the upper frequencies (-16 db at 15.5 GHz) due to surface tolerance effects.

Beamwidth data shown in Figure 45 corresponds closely to predicted values. The major diagonal of the hexagonal aperture

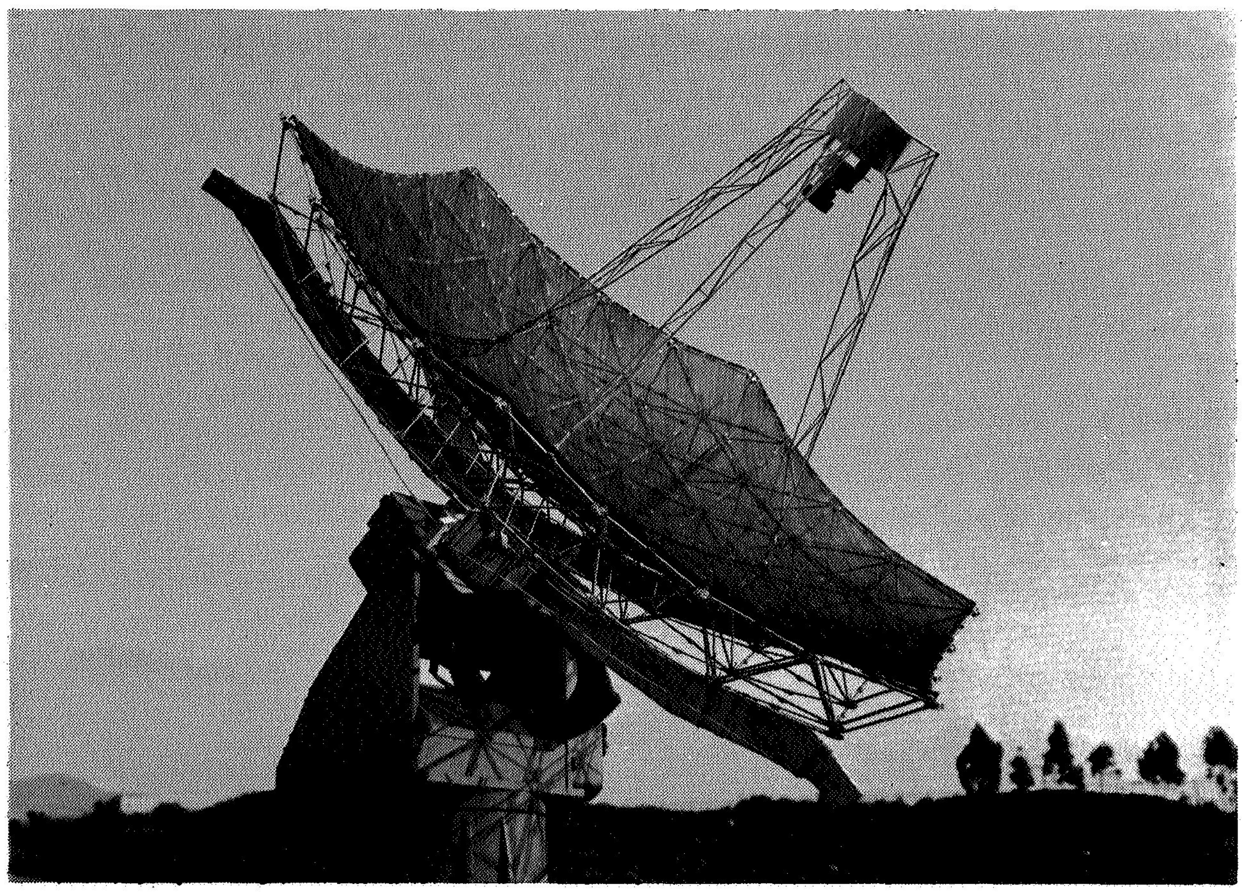

Figure 43

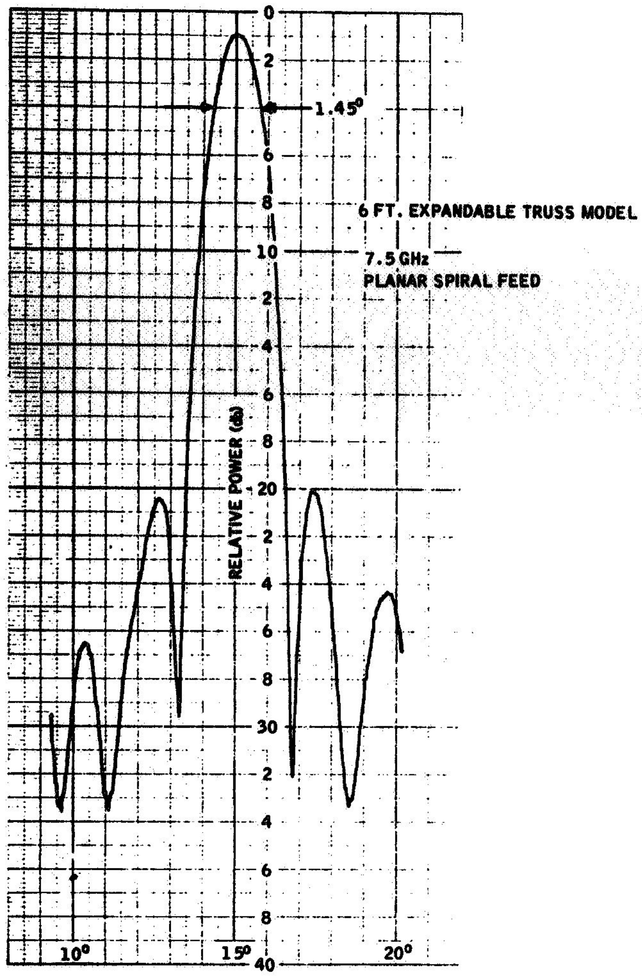

Figure 44

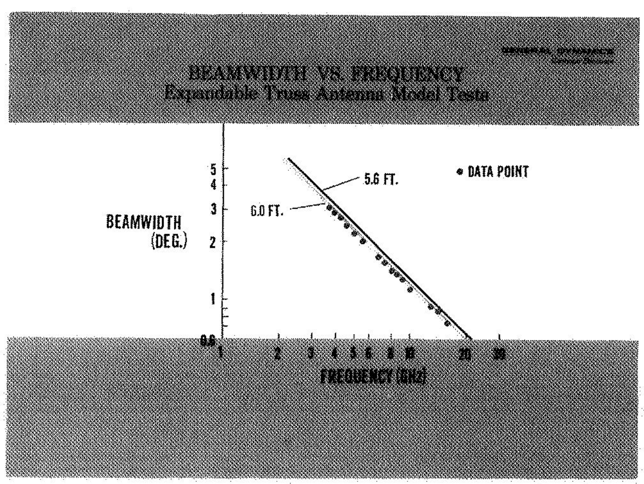

Figure 45

was 6.2 ft. for an effective circular diameter of 5.6 ft. Best fit of the data points corresponds to a six-foot diameter antenna.

Gain data is given in Figure 46. An ideal parabolic antenna having an efficiency of 55 per cent and diameter of 5.6 ft. is shown for comparison. Surface tolerance effects become more pronounced at the upper frequencies in terms of consistent gain loss. A maximum gain frequency of 25 GHz is estimated for the model antenna, based on the existing RF gain data. This would arise from an approximate RMS surface tolerance of 0.040 in.

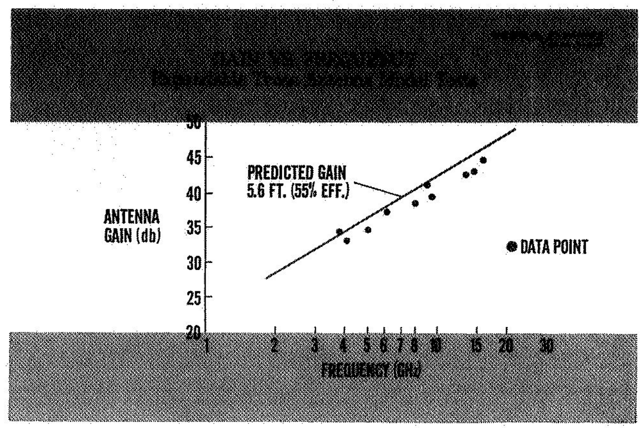

Figure 46

An important aspect of the test is that excellent gain and pattern data was attained on a manually constructed antenna — one built without the aid of precision tooling. No attempt was made to improve tolerances or to optimize to the best-fit parabola by feed positioning. Part of the 0.040 RMS achieved is due to the built-in 0.015 hexagonal flats used to approximate the parabola.

Mesh Reflectivity Tests

Reflectivity tests on two mesh materials were conducted during the study, using silver-coated nylon and Chromel-R. A complete physical description and evaluation of the materials are presented in an earlier section of this report.

Measurements of silver-coated nylon were necessary as this material was used on the six-foot RF test model. Any loss in surface reflectivity decreased antenna gain values. Chromel R reflectivity values were of interest because of its application to the full-scale large erectable space antenna. Relative reflectivity values between the two materials were also of interest, since Chromel-R is considerably more expensive than the silvered nylon.

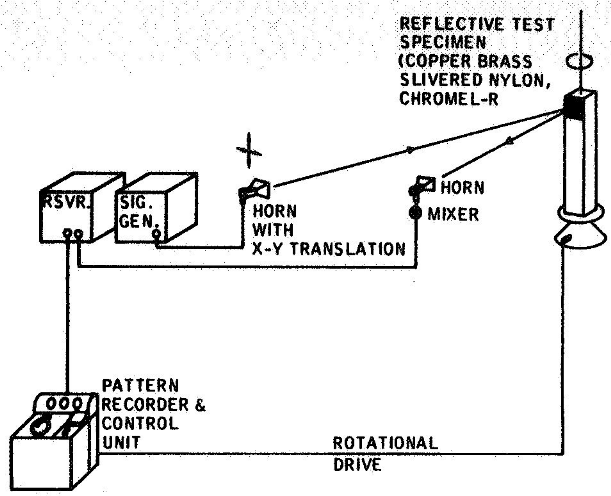

Figure 47

A measurement diagram for the reflectivity test is shown in Figure 47. In this scheme, the quantity of reflected energy from a given size mesh specimen is compared with that from a known conductor (copper, brass, aluminum) of identical size. The comparison is made from maximum amplitude responses recorded on polar graph paper. Transmission through the mesh or absorption by the mesh reduces the response.

Results are summarized in Figure 48. A brass specimen was also used in the test for a second reference material, but results were not plotted. The significant points of the curve are that both materials are satisfactory for reflectors through the limits of the test (through 15 GHz). Conductor spacing at 15 GHz is approximately one-tenth wavelength so that leakage is not significant.

The slight advantage shown at the higher frequencies by the silvered nylon may be due to the increased mesh density (5 to 10 per cent) of the sample.

Based on these tests, only negligible 0.1 to 0.2 db loss could be attributed to the silvered nylon mesh reflectivity in the absolute gain computations. Both materials are readily acceptable as reflectance mesh for the antenna.

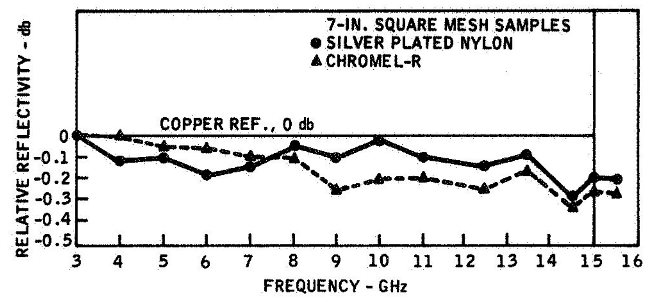

Figure 48

ASTRONAUT EQUIPMENT

To perform the tasks outlined in Figure 49 the astronaut will have a command console in the feed-electronic compartment. He will use the laser surface measurement system to evaluate the surface contour, recommend corrections, and decide what action to take. He will steer the antenna to acquire the transmitter and monitor pattern measurements throughout the test. Aided by ground control, he will decide which sections of the patterns test should be repeated. In the noise and pointing tests, he will steer the antenna and initiate lock-on to ground, satellite, and celestial targets. He will backcheck the attitude sensor equipment with position fixes at critical acquisition phases.

His potential EVA tools and spare parts are listed in Figure 50. A low-reaction hand torque gun will be used to make mesh corrections. C-clamps have broad appli-

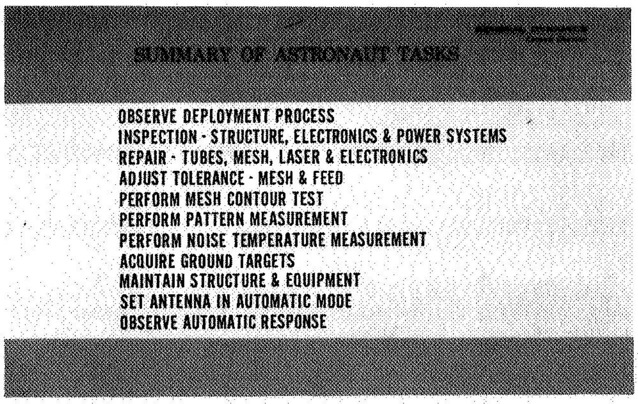

Figure 49

cation in positioning material to make adjustments or repairs. Wire and coaxial splicers are need should deployment or boost vibration damage the lines from the peripherally mounted equipment to the electronic compartment. Metal and mesh cutters could be used to release a damaged truss tube. Redundance of the truss will

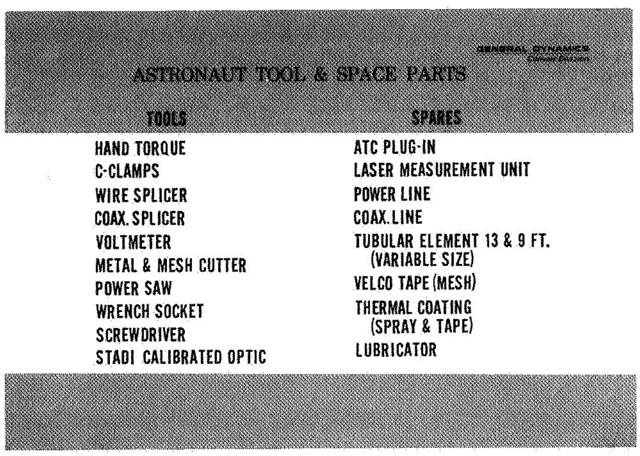

Figure 50

allow any one of the six elements in a hexagonal assembly to be removed without impairing the structural integrity of the antenna. A stadi optic could be used to approximate distances and make measurements of the truss and mesh. Each ACS engine module can be removed and a new module plugged in.

The laser mounts on a hatch in the electronic compartment can be removed for repair or replacement by a spare. Power and coaxial line replacements may be stored on the side of the electronic compartment. A telescopic tubular element spare can be used to replace any damaged tubes or as a test of EVA dexterity in a simulated repair.

Tests made on the mesh show that Velvco tape is ideal for joining a damaged area. If surfaces are marred during boost or deployment, the thermal coating would be repaired with tape during the EVA inspection. Lubrication would be useful for the tube and feed hinges and the adjustment system.

Simulation of the feed-electronic compartment and a EVA simulator on a hexagonal element of the reflector are needed to determine the feasibility of various crew tasks. Once the tasks are established, mockups will be used for training.

Astronaut Training and Simulation Aids

Astronaut training requirements are outlined in Figure 51. Simulation aids will include: (1) a mockup of the electronic-feed compartment with simulation of all test functions, including a pattern measurement system. Malfunctions may also be programmed into the mockup and tests to prepare the astronaut for potential problems. (2) Hexagonal structural element, (Figure 52) for deployment and underwater EVA simulation of tube repair and mesh adjustment. (3) Feed mockup for RF testing and underwater EVA repair simulation.

Training will also take place in the actual structure during fabrication, test and after completion of the prototype. The prototype will be updated to serve as a training aid during flight hardware assembly.

WEIGHT SUMMARY

The synchronous orbit, 100-ft. diameter experiment total weight (Figure 53) is

ASTRONAUT TRAINING

120 HR. — COURSE IN PARABOLOID ANTENNA THEORY & LASER MEASURING UNIT

120 HR. — EQUIPMENT USAGE

120 HR. — MALFUNCTION DETECTION, ANALYSIS & REPAIR TECHNIQUES

80 HR. — SAFETY PROCEDURES

TOTAL TIME REQUIRED: 800 HR.

AT LEAST 3 TO 6 ASTRONAUTS
ARE TRAINED AT SAME TIME

TASK SIMULATION

1. LASER MEASUREMENT UNIT TESTS
   EVALUATE DATA
   REPAIR EQUIPMENT
   FEED BORESIGHTING
2. RF TESTS:
   PATTERN MEASUREMENT
   GAIN MEASUREMENT
   ALIGNMENT
   CALIBRATION
   DATA ANALYSIS
   NOISE MEASUREMENT
   TRANSMISSION TEST
3. EVA STRUCTURAL TASKS:
   DETECTION & REPAIR OF MALFUNCTION IN DEPLOYMENT
   ADJUSTMENT OF REFLECTOR MESH
   ELECTRICAL CONNECTIONS
   INSTALLATION & CHANGE OF COMPONENTS
   INSPECTION
   MAINTENANCE
   TOOL HANDLING
4. POINTING TESTS
   ACQUIRE GROUND STATION
   ACQUIRE SATELLITE
   ACQUIRE CELESTIAL OBJECT 240 HR.

MISSION SIMULATION & FAMILIARIZATION
SEQUENTIAL STEPS IN MISSION PROCEDURE FOR DEPLOYMENT & INITIAL OPERATION OF PARABOLIC ANTENNA EXPERIMENT 120 HR.

Figure 51

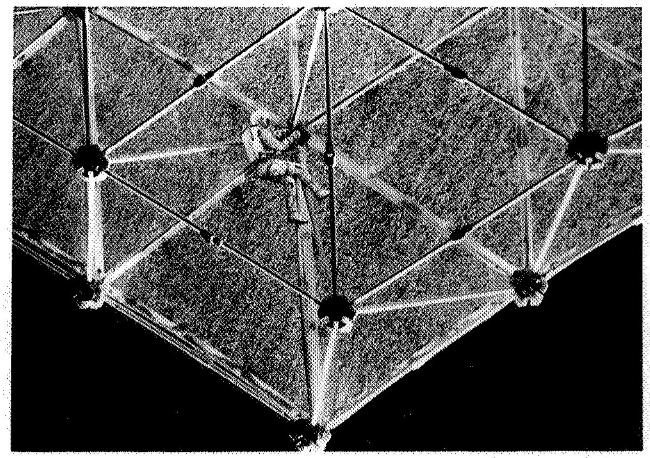

Figure 52

5,523 lb., in which the two heaviest systems are power and attitude control. A 300-mi. orbit experiment would weigh approximately 6,100 lb. due to increased torque and orbit-keeping requirements. Reflector weight is a small part of the total experiment at 0.10 lb./sq.ft. of aperture. Reflector weight could be reduced to 0.060 lb./sq.ft. if beryllium tubing is used. Since ample payload is available with the Saturn V launch, most systems have been selected for maximum reliability and least cost rather than weight. A Saturn IB launch with an Apollo would require a velocity input by the Service Module to move the manned experiment into a 300-mi. orbit. If weight saving becomes necessary due to addition of other experiments, electrical power and attitude control systems can be reduced with an accompanying reduction in antenna experiment information.

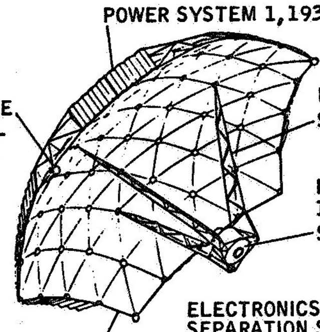

Figure 53

RF BEAM STEERING

Beam steering concepts investigated in this report were applied to the currently configured 100-ft. diameter parabolic truss with a focal length of 40 ft. A larger f/D ratio gives improved beam steering performance as shown in Figures 54 and 55. Consequently, several additional antenna configurations were derived having a unity f/D ratio.

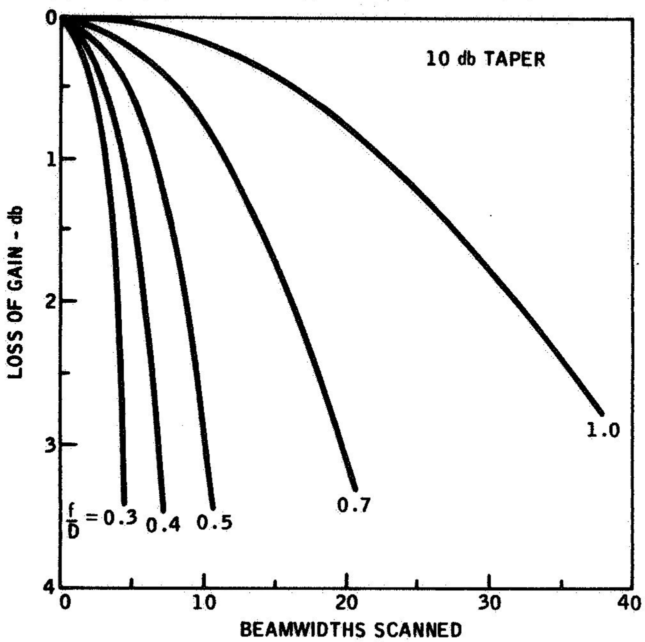

Figure 54

A number of beam steering techniques were analyzed, including feed translation, switched matrix feed, reflector tilt, subreflector tilt, subreflector translation, and spherical antennas.

Several conclusions of the study are: The parabolic antenna with a f/D ratio of 0.4 was limited to a scan angle of approximately four beamwidths by RF performance degradation. The simplicity of the Newtonian feed is preferred over the Cassegrain. The translated feed gives a fine beam position control with less microwave component loss than the switched feed matrix. Crossover loss of several decibels can occur in the switched feed systems.

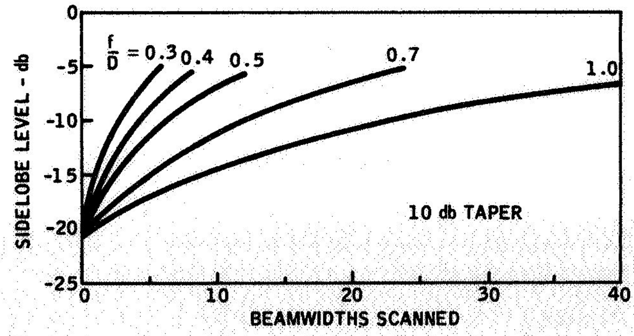

Figure 55

If a Cassegrain system is required, the least complex scheme is the rotating subreflector.

Torque f/D ratios of the order of unity are best scanned by reflector tilt rather than feed displacement.

Several mechanical concepts used to steer the feed and reflector are illustrated in Volume IV.

RELIABILITY

With the experiment designed to use man in each phase, total reliability can be increased from 0.963 for an unmanned system to 0.998. (Figure 56). Reliability for successful deployment of the feed and reflector is 0.988. Calculations are based on aircraft control systems that use multiple-pushrod, hinged elements. Five-year reliability, as shown by Figure 57, is primarily diminished by the attitude control and power systems. Once deployed, the reflector, with insignificant meteoroid punctures and thermal coating degradation, is relatively unchanged.

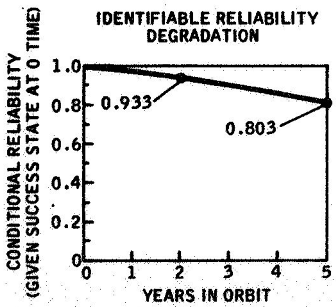

SUBSYSTEM	2 YR.	5 YR.
ANTENNA	1.0	1.0
ELECTRICAL	0.998	0.984
ATTITUDE CONTROL	0.935	0.821
DATA	0.999	0.995
RF	0.999	0.998
TOTAL	0.933	0.803

Figure 56

FABRICATION AND TEST

Figure 58 illustrates the proposed sequence. Four basic items — reflector, feed support, feed and electronic compartment, and the boost and transportation pallet — are fabricated. Upon completion of the basic truss of the reflector and feed, the antenna will be assembled in the packaged condition (3).

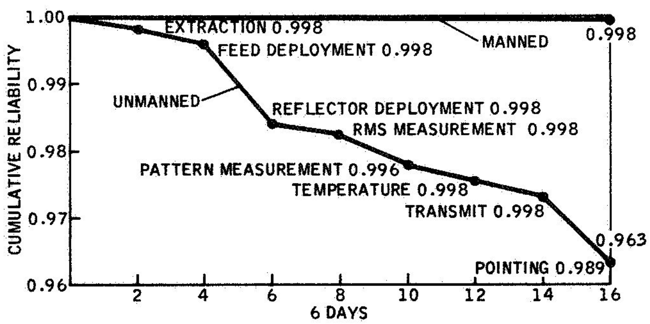

Figure 57

A fit check will be made in the pallet. A negator spring system will ride a trolley rail carrying the weight of each spider section to simulate zero gravity during deployment (4). The deployed antenna will then be vibrated (5) to determine the primary modes. Disassembly and installation of the mesh (6) on the reflector and equipment in the compartment follow. A separate packaging and deployment of the reflector (7) (8) will check out the system with the mesh on. The re-packaged complete assembly will then be vibrated to (9) boost loading condition and the full flight sequence simulated (10).

RF testing will be performed on a scale antenna. A 30 to 50-mile test range would be required for the full size antenna. Since all testing is nondestructive, a similar sequence of operations will be performed on the flight antenna for qualification.

Figure 59 illustrates the fabrication jig. The zero-g trolley system will be on a spider web network above the antenna. Temperature control of $\pm 2^{o}$ is desirable to prevent tolerance buildup. All assembly, packaging, and testing will be done in the jig area.

COST AND SCHEDULE

Program Phase C entails detail design and prototype test. A schedule of the major tasks is given in Figure 60. Fabrication and test of the prototype will be followed by a short design optimization period before fabrication and qualification of the flight experiment. Prototype testing will be completed in 21 months. Launch of the experiment can take place 34 months from go-ahead.

Cost of the complete experiment, including development, ground and training equipment, prototype fabrication and test, and one flight article, would be $27.3 million. Figure 61 outlines the fiscal funding requirements. Major costs are in the power ($4.4M) and attitude control system ($4.5M). The erectable structure system including the full test cycle, costs $2.65M. Phase C separately with minimum purchase of power and attitude control system components would cost $10M. A recurring cost of $11.29 for an additional flight vehicle includes all of the experiment and system components.

A completed NASA 1347 form is supplied in Volume IV of this report.

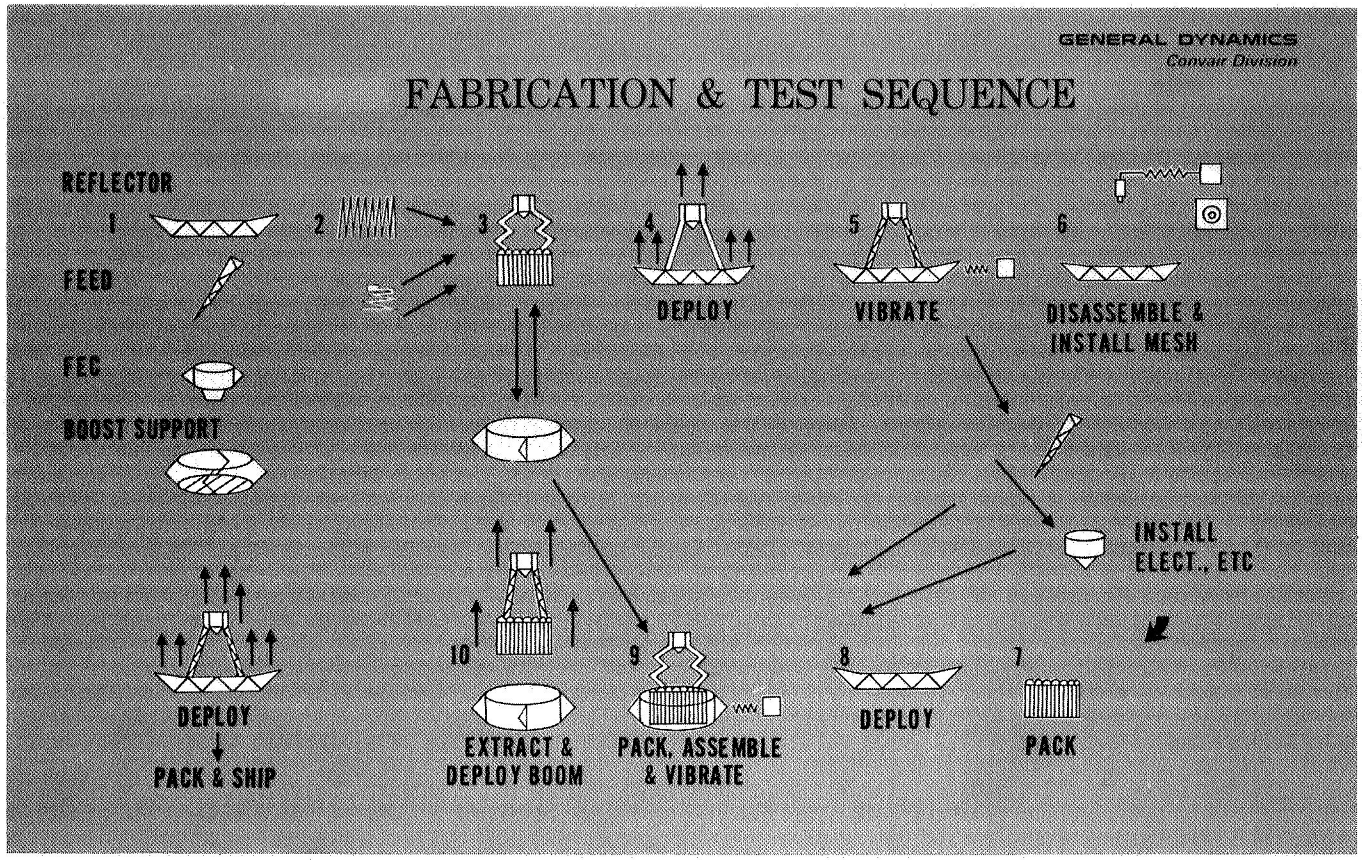

Figure 58

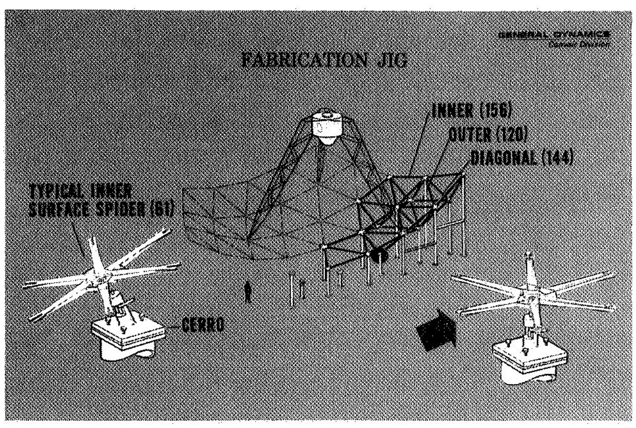

Figure 59

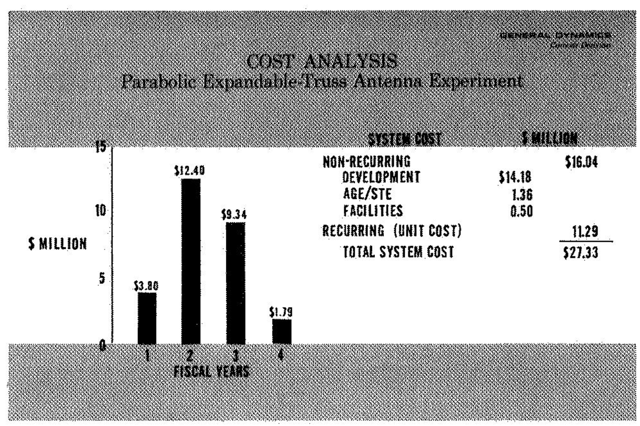

Figure 61

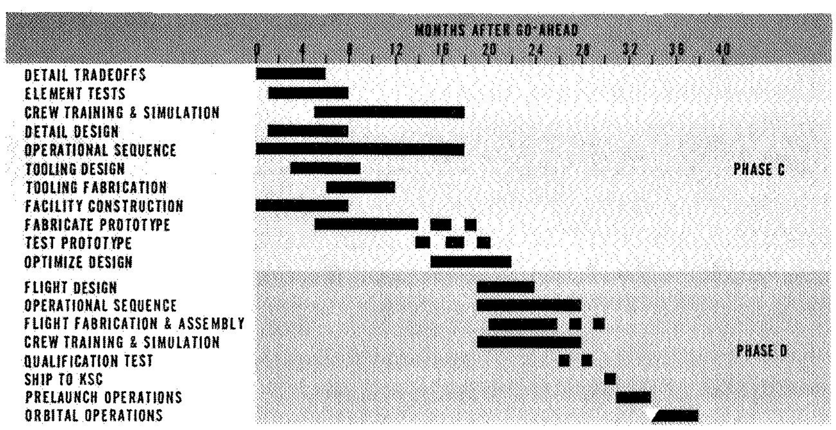

Figure 60. Development schedule

DEVELOPMENT TASKS

Primary development tasks that require particular effort are itemized in Figure 62.

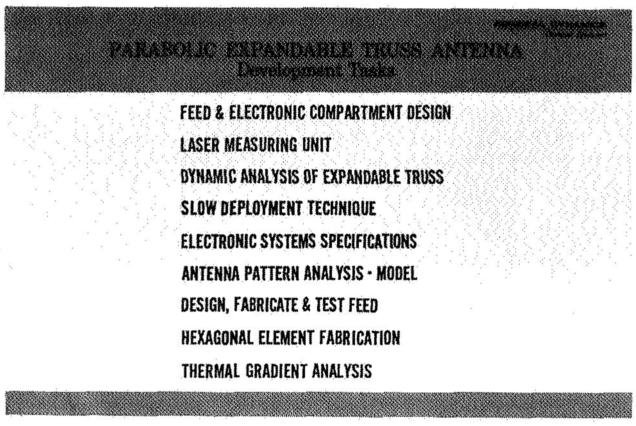

Figure 62.

Feed-electronic compartment design requires integration of the equipment into the eight-foot diameter pressurized capsule. Life support units similar to those in the LM or Multiple Docking Adaptor will be examined to determine their applicability.

The laser measurement unit is within the state of art of laser technology but has not previously been assembled to perform the proposed measurement task. Development may be divided into three parts: laser system, scanning system, and software printout system.

Transient dynamic analysis during deployment must be developed so that spring size and type may be varied to provide reliable deployment with minimum loads on the peripherally mounted components. Model tests will be performed to substantiate the analysis.

Slow deployment is feasible, but details must be worked out. Many schemes of controlling deployment have been suggested. The best of these concepts must be evaluated and tests made on the available model to demonstrate the design.

General characteristics of the electronic system have been determined in the current task. The next step is a detail matching of the requirements with available ground and space-proven equipment.

Antenna pattern analysis was carried up to 15 GHz on the model. Further testing up to 30 GHz is required in addition to vacuum and thermal cycle test of the RF mesh. Effects of the Apollo blockage and reflectance of the telemetry antennas against the large antenna must also be evaluated.

The proposed conical feed has an erectable, low-frequency feed. This structure should be developed and the feeds illumination characteristics determined.

Fabrication of a full-scale, hexagonal element of the mesh with the adjustment system would substantiate the design concept and work out "bugs" before full-scale fabrication is attempted. Deployment, dynamic, thermal, and human factors evaluation tests could be performed on the element and the results integrated into the prototype design.

Thermal gradients through the tubular structure and mesh at various sun angles necessitate a more detailed analysis to substantiate the anticipated temperatures. Temperature distribution around perforated tubes and end fittings should be tested in a vacuum chamber.